Quantitative analysis of the effect of disorder-induced mode coupling on infrared absorption in silica

C. T. Kirk
Lincoln Laboratory, Massachusetts Institute of Technology, P.O. Box 73, Lexington, Massachusetts 02173-0073
(Received 4 January 1988)

The infrared-absorption spectrum of a-SiO_2 is analyzed in terms of its transverse-optic (TO) and longitudinal-optic (LO) vibrational modes. It is shown that the independent-oscillator model for the a-SiO_2 dielectric function fails to yield a consistent value of mode strength for the optically active oxygen asymmetric stretch (AS_1) TO mode at 1076 cm^{-1} (in-phase motion of adjacent oxygen atoms) when different but equivalent methods of measurement and analysis are used. This inconsistency is resolved by introducing disorder-induced mechanical coupling between the AS_1 mode and the relatively optically inactive oxygen asymmetric stretch (AS_2) mode (out-of-phase motion of adjacent oxygen atoms) into the oscillator model. Coupled AS_1- and AS_2-mode LO-TO frequency pairs are experimentally observed as peaks at approximately 1256–1076 cm^{-1} and 1160–1200 cm^{-1}, respectively, in oblique-incidence p-polarized absorption spectra of thin a-SiO_2 films grown thermally on c-Si wafers. Additionally, two other LO-TO-mode pairs are observed in these spectra as absorption peaks at approximately 820–810 cm^{-1} and 507–457 cm^{-1}. The simplest form of the coupled-mode model consistent with experiment is found to be one in which the AS_1-mode LO-TO frequency splitting is due to the AS_1 transverse effective charge and the AS_2-mode LO-TO splitting is due to the mechanical coupling between these two modes and not to the AS_2 transverse effective charge, which is negligibly small. The AS_2 TO and the AS_1 LO modes found at approximately 1200 and 1256 cm^{-1}, respectively, are shown to be consistent with experimental mode strengths and with the analytic requirements that all LO and TO modes be interspersed and that, as a result of lying between the AS_1-mode LO-TO pair frequencies, the AS_2-mode LO-TO frequency splitting be inverted. Comparison of these experimental LO-TO-mode pair frequencies with the vibrational density of states (VDOS) spectrum of a-SiO_2 shows that the TO absorption peaks correspond quite well with the VDOS spectral peaks, whereas the LO absorption peaks do not appear to exhibit any such correspondence.

I. INTRODUCTION

This paper is concerned with the quantitative interpretation of the infrared absorption of silica or amorphous silicon dioxide (a-SiO_2). There has been a great deal of research directed toward interpreting the features in the infrared spectrum of a-SiO_2 in terms of the local vibrational modes associated with this tetrahedral glass.[1] With the discovery of the longitudinal-optic–transverse-optic (LO-TO) frequency splitting of the vibrational modes in tetrahedral glasses and a-SiO_2 in particular,[2] certain inconsistencies arose concerning a-SiO_2 as to the frequency assignment of its highest-frequency LO mode[2,3] and as to the correct determination of the absorption strength of the associated TO mode.[4] This paper shows how a reinterpretation of the infrared spectrum to include an additional LO-TO frequency-split mode can remove these inconsistencies in frequency assignment and allow the correct determination of TO-mode strengths in a-SiO_2.

Figure 1 shows a typical infrared TO absorption spectrum for a-SiO_2 as obtained from a 100-nm-thick oxide film grown thermally at 1000 °C on (100) silicon. Each of the three major TO absorption bands shown in the figure can be characterized in terms of a particular vibrational mode of the oxygen (O) atoms with respect to the silicon (Si) atom pairs which they bridge. Rocking (R) of the O atom about an axis through the two Si atoms characterizes the vibrational behavior of the lowest-frequency TO band centered at $\approx$457 cm^{-1}. Symmetrical stretching (SS) of the O atom along a line bisecting the axis formed by the two Si atoms characterizes the vibrational mode of the middle TO band centered at $\approx$810 cm^{-1}. The remaining TO band and its high-frequency shoulder are due to an asymmetrical stretch (AS) motion in which the O atom moves back and forth along a line parallel to the axis through the two Si atoms. The AS motion actually gives rise to two vibrational modes: (1) an AS_1 mode in which adjacent O atoms execute the AS motion in phase with each other, and (2) an AS_2 mode in which adjacent O atoms execute the AS motion 180° out of phase with each other.[5,6] The AS_1 mode is characteristic of the vibrational behavior of the TO band centered at $\approx$1076 cm^{-1} and it will be shown that the AS_2 mode typifies the behavior of the shoulder centered at $\approx$1200 cm^{-1}.

Paired with each of these four TO modes is a LO mode. In general, the LO vibrational motion is not the same as its paired TO mode, and their frequencies are different, the LO mode being the higher. The splitting of a vibrational mode of a material into an LO-TO pair is a

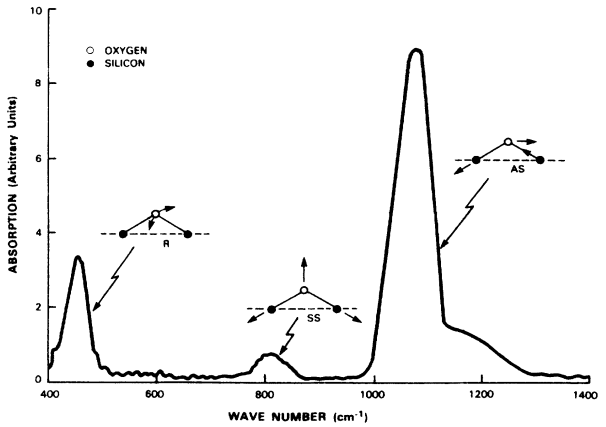

FIG. 1. Infrared TO absorption spectrum for a-SiO_2 obtained from a 100-nm-thick oxide film grown thermally at 1000 °C on (100) silicon showing the local vibrational motions of rocking (R), symmetrical stretching (SS), and asymmetrical stretching (AS) of the oxygen atoms (○) with respect to the silicon atom (●) pairs which they bridge that are associated with the three major features of the absorption spectrum.

direct result of the interaction of the vibrational motion of the mode with the material's electromagnetic field through the electric charge on the vibrating atoms. LO modes are not observed in normal-incidence infrared-absorption spectra such as that shown for a-SiO_2 in Fig. 1 since they do not interact directly with light. However, they can be observed in oblique-incidence absorption spectra[7,8] due to the Berreman effect.[9]

According to classical optical-dispersion theory[10] the infrared-absorption spectrum for a-SiO_2 shown in Fig. 1 can be interpreted and modeled in terms of a collected set of independent harmonic electric-dipole oscillators, each oscillator being characterized by the strength and the density of a different TO mode.[11–13] Basically, there are two ways in which to determine the mode strength of an oscillator: either by direct measurement from an infrared spectrum or by calculation from the measured LO and TO frequencies of all of the LO-TO-mode pairs. Either way the strengths should be the same. In practice, however, this has not proved to be the case. As described in Sec. III C, reported strengths for the 1076-cm^{-1} mode of a-SiO_2 measured directly from infrared spectra are lower than those calculated from the reported LO-TO-pair frequencies of a-SiO_2 by 30–40%, depending on the references used. This inconsistency is further aggravated by the fact that there is a disagreement in the literature as to the frequency of the LO mode to be paired with the AS_1 TO mode at 1076 cm^{-1}.[2,3]

It is the intention of this paper to show how these discrepancies can be resolved in a relatively simple manner. This will be accomplished by introducing mode coupling into the classical oscillator model for optical dispersion described above. Discrepancies in the determination of the 1076-cm^{-1} TO-mode strength of a-SiO_2 and in the frequency of the associated LO mode will be shown to be due to a failure to take into account the coupling that is proposed to occur in a-SiO_2 between the AS_1 and AS_2 modes.

This paper is organized as follows: In Sec. II we describe the optical properties of the classical independent-oscillator model of a dielectric. Measurement and analysis of the absorption spectrum of a thin oxide film grown on a silicon substrate are described in terms of this model. The strength of the film's 1076-cm^{-1} vibrational mode is defined and calculated and comparison is made to mode strengths obtained by other workers using different methods of measurement and analysis and different forms of SiO_2. In Sec. III coupled-mode dielectric theory is developed for two modes. In Sec. IV we describe both the experimental procedures for making and measuring thin films of a-SiO_2 and the analytical procedures for obtaining the experimental results used to test the coupled-mode dielectric theory. In Sec. V the coupled-mode dielectric theory developed in Sec. III is applied to the analysis of the absorption spectra of thin oxide films on silicon. Section VI is a discussion as to how mode coupling explains and resolves the discrepancies associated with the measurement of the a-SiO_2 1076-cm^{-1} TO-mode strength and the frequency of its paired LO mode. Conclusions drawn from this infrared study of LO and TO modes in thin a-SiO_2 films are described in Sec. VII.

II. CLASSICAL INDEPENDENT-OSCILLATOR MODEL

A. Dispersion relations

The optical behavior of a dielectric material can be described by Maxwell's equations and the material's dielectric function $\epsilon(\nu)$, where ν is the optical frequency. From dispersion theory, a dielectric material whose optical vibrational modes can be characterized as an assembly of independent electric-dipole oscillators has an $\epsilon(\nu)$ of the form[14]

$$\epsilon(\nu)=\epsilon_\infty+\sum_j \frac{4\pi F_j}{\nu_{Tj}^2-\nu^2-i\nu\gamma_{Tj}} , \tag{1}$$

where ϵ_∞ is the optical or high-frequency dielectric constant due to the electronic polarizability of the material, and F_j, ν_{Tj}, and γ_{Tj} are the strength, vibrational frequency, and Lorentzian width, respectively, of the material's jth-mode TO oscillator. These last three quantities serve to characterize the poles of $\epsilon(\nu)$ which give rise to the TO-mode absorption lines. The mode strength of the jth TO oscillator, defined by F_j, can be expressed in terms of physical parameters of the dielectric material by the relation[14]

$$F_j=e_j^{*2}/4\pi^2\bar{M}_j\Omega_j , \tag{2}$$

where e_j^* is the transverse effective dipolar charge, $\bar{M}_j$ is the oscillator reduced mass, and Ω_j is the unit volume of the jth TO-mode dipole oscillator. Despite its simplicity, Eq. (1) often reproduces the ir reflectivity and transmission spectra of dielectric materials quite well.

Equivalently, the dielectric function can be expressed in the alternative form[15]

$$\epsilon(\nu)=\epsilon_\infty \prod_j \frac{\nu_{Lj}^2-\nu^2-i\nu\gamma_{Lj}}{\nu_{Tj}^2-\nu^2-i\nu\gamma_{Tj}} , \tag{3}$$

where ν_{Lj} and γ_{Lj} are the vibrational frequency and Lorentzian width, respectively, of the dielectric's jth LO-mode oscillators. Accordingly, the LO modes are related to the zeros of the dielectric function. Since Eqs. (1) and (3) are equivalent, in principle, ν_{Lj} and γ_{Lj} can be expressed in terms of F_j, ν_{Tj}, and γ_{Tj}. The procedure for obtaining these relationships requires factoring a polynomial of degree $2N$, where N is the number of modes, and it is not practical to do so for a multimode system. However, in the limit of zero damping ($\gamma_{Tj}=\gamma_{Lj}=0$), a relatively simple relationship between the jth-mode oscillator strength F_j and the LO and TO modes of the dielectric material can be found, of the form[16]

$$4\pi F_j=\epsilon_\infty(\nu_{Lj}^2-\nu_{Tj}^2)\prod_{\substack{k\ (\neq j)\\ (j=1,\ldots,N)}}^{N}\frac{\nu_{Lk}^2-\nu_{Tj}^2}{\nu_{Tk}^2-\nu_{Tj}^2} , \tag{4}$$

which can be used to obtain estimates of the F_j's.

Strictly speaking, Eqs. (1)–(4) apply only to crystalline materials of orthorhombic or higher symmetry with a discrete vibrational density of states (VDOS). The amorphous structure of a-SiO_2 can be accommodated within the theoretical framework of Eq. (1) by changing each (jth) mode of the discrete VDOS spectrum of α-quartz into a Gaussian-like continuous frequency distribution of jth-mode oscillators peaked about some center TO frequency ν_{Tj}. Accordingly, the dielectric function for a-SiO_2 should be strictly of the type[11–13]

$$\epsilon(\nu)=\epsilon_\infty+\sum_j\int_0^\infty \frac{4\pi F_j(\xi)}{\xi^2-\nu^2-i\nu\gamma_j}g_j(\xi-\nu_{Tj})d\xi , \tag{5}$$

where g_j is the normalized frequency density distribution of the jth-mode oscillators, and the jth integrated mode strength is

$$\langle F_j\rangle=\int_0^\infty F_j(\xi)g_j(\xi-\nu_{Tj})d\xi . \tag{6}$$

In general, the dielectric function ϵ is complex and its real and imaginary parts, ϵ' and ϵ'', respectively, are related causally through the Kramers-Krönig dispersion equations,

$$\epsilon'(\nu)-\epsilon_\infty=\frac{2}{\pi}\mathrm{P}\int_0^\infty\frac{\xi\epsilon''(\xi)}{\xi^2-\nu^2}d\xi \tag{7}$$

and

$$\epsilon''(\nu)=-\frac{2\nu}{\pi}\mathrm{P}\int_0^\infty\frac{\epsilon'(\xi)-\epsilon_\infty}{\xi^2-\nu^2}d\xi , \tag{8}$$

where ϵ' and ϵ'' are given by the real and imaginary parts, respectively, of either Eq. (1), (3), or (5).

B. Sum rules

Mode strength F_j can be expressed in terms of the dielectric loss function $\epsilon''(\nu)$ as a sum rule by making use of Eq. (7). Upon taking ν in Eq. (7) to be much larger than some cutoff frequency ν_c such that $\epsilon''(\nu)=0$ for $\nu>\nu_c$ (i.e., there is no absorption due to the vibrational modes for frequencies higher than ν_c), it can be deduced that

$$\epsilon'(\nu)-\epsilon_\infty=-\frac{2}{\pi\nu^2}\int_0^\infty\xi\epsilon''(\xi)d\xi \quad (\nu\gg\nu_c) . \tag{9}$$

Under the same conditions, viz., $\epsilon''(\nu)=0$; $\nu>\nu_c$, the dielectric function, as described by Eq. (1), becomes

$$\epsilon'(\nu)-\epsilon_\infty=-\frac{1}{\nu^2}\sum_j 4\pi F_j \quad (\nu\gg\nu_c) . \tag{10}$$

The definition

$$\epsilon''(\nu)=\sum_j\epsilon_j''(\nu) \tag{11}$$

follows directly from Eq. (1), where ϵ_j'' is that part of the dielectric-loss function ϵ'' due only to the jth vibrational mode. By combining Eqs. (9)–(11), and then letting $\xi\to\nu$, a sum rule can be obtained, of the form

$$4\pi F_j=\frac{2}{\pi}\int_0^\infty\nu\epsilon_j''(\nu)d\nu , \tag{12a}$$

where the integrand involves only the dielectric-loss function due to the jth vibrational mode. This sum rule is important in that it allows the F_j's to be determined directly from experimental data.

In a similar manner, the dielectric function for Gaussian-broadened modes [Eq. (5)] gives rise to the sum rule

$$4\pi\langle F_j\rangle=\frac{2}{\pi}\int_0^\infty\nu\epsilon_j''(\nu)d\nu , \tag{12b}$$

where again it is noted that the integrand involves only that part of $\epsilon''(\nu)$ arising from the jth vibrational mode. While Eqs. (12a) and (12b) are formally identical, numerical values for F_j and $\langle F_j\rangle$ can differ due to differences in e_j^* and Ω_j for the crystalline and amorphous forms of a material and, in the case of amorphous material, as a result of the convolution of these quantities with the distribution function $g_j(\nu)$. This distinction between F_j and $\langle F_j\rangle$ as the respective mode strengths of crystalline and amorphous materials really occurs with the choice of the dispersion relation, Eq. (1) or (5), used in order to determine ϵ_j''. Accordingly, in the remainder of the paper the symbolic distinction will not be made; F_j will be used for both types of mode strengths, relying on the reader to make the distinction from the manner in which ϵ_j'' is determined.

C. Mode strengths

Experimental determination of the F_j's in bulk materials are usually made using either reflection or Raman spectroscopy. In thin film materials, the F_j's can be determined using either transmission or reflection spectroscopy.[13,17] In the case of bulk materials, experimental infrared-reflectivity spectra R are fitted using[14]

$$R=|(\sqrt{\epsilon}-1)/(\sqrt{\epsilon}+1)|^2 , \tag{13}$$

together with Eq. (1) or (5), depending on the crystallinity

of the material, for a direct determination of the F_j's. For purely crystalline materials, Eq. (3) can be used in conjunction with Eq. (13) to fit the reflectivity data and the F_j's estimated subsequently using Eq. (4). Values of F_j can be estimated directly from the Raman spectra of materials with the aid of Eq. (4), provided the LO and TO spectral frequencies can be correctly identified.

Information concerning the F_j's of thin-film materials is quite easily obtained from transmission spectra for those oscillator modes whose absorption peaks do not overlap or can otherwise be separated out. Maeda *et al.*[18] have analyzed the problem of transmission through very thin films on thick dielectric substrates. They considered the case of a single film of thickness d supported by a substrate of thickness much greater than the wavelengths λ of the incident radiation, of refractive index n, and of negligible reflectance at the substrate-air interface. They showed that in the limiting case of zero film thickness, the film's dielectric-loss function $\epsilon''(\nu)$ is related to the transmitted intensity through the film and the substrate, $I(\nu)$, by an equation of the form

$$\nu\epsilon''(\nu)=\lim_{d\to 0}\left[\frac{1}{2\pi[2/(1+n)]d}\right]\ln\left[\frac{I_0'(\nu)}{I(\nu)}\right], \tag{14}$$

where $I_0'(\nu)$ is the transmitted intensity of the radiation through the substrate alone.

By following Maeda, a limit relation between $\nu\epsilon_j''(\nu)$ and the transmitted intensity affected only by the jth-mode oscillators, $I_j(\nu)$, can be derived for the experimental film arrangement in this paper, which consists of a thick ($\gg\lambda$) silicon substrate optically polished on both sides and covered on each side with identical thermally grown films of oxide. This relation can be shown to have the form

$$\nu\epsilon_j''(\nu)=\lim_{d\to 0}\left[\frac{1}{2\pi[(3+n_{\mathrm{Si}}^2)/(1+n_{\mathrm{Si}}^2)]d}\right]\ln\left[\frac{I_0'(\nu)}{I_j(\nu)}\right], \tag{15}$$

where $I_0'(\nu)$ now refers to the transmitted intensity through the bare silicon wafer and n_{Si} is the silicon optical index of refraction. By combining Eqs. (12) and (15) to eliminate $\nu\epsilon_j''(\nu)$, an expression for F_j is obtained in the limit form

$$F_j=\lim_{d\to 0}\left[\frac{1}{4\pi^3[(3+n_{\mathrm{Si}}^2)/(1+n_{\mathrm{Si}}^2)]d}\right]\times\int_0^\infty\ln\left[\frac{I_0'(\nu)}{I_j(\nu)}\right]d\nu, \tag{16}$$

which relates F_j to the apparent integrated absorbance of the film's jth TO-mode oscillators defined by $d^{-1}\int_0^\infty\ln[I_0'(\nu)/I_j(\nu)]d\nu$.

As Eqs. (1), (4), (5), (12), and (16) suggest, experimental determination of F_j can be accomplished in a number of ways. In accordance with Eq. (2), the values obtained should be in reasonable agreement once differences in density due to the different forms of the material are taken into account, and assuming all other pertinent material parameters remain the same. Table I shows a comparison of values of F_1, the 1076-cm^{-1} AS_1 TO-mode strength for a-SiO_2, either taken from the literature or calculated from literature data using the equations for F_j described above. To facilitate comparison, values of F_1 shown in Table I are scaled to the density of α-quartz. From Eq. (2), this density scale factor is seen to be just the ratio of the α-quartz density to the density of the particular form of a-SiO_2 being scaled. Values for the density η of the various forms of SiO_2 pertinent to this paper are given in Table I.

Various methods are used to obtain the density scaled values of F_1 listed in Table I. Spitzer *et al.*[14] obtained their value for F_1 (Ref. 19) by using Eq. (13) to fit Eq. (1) to their reflection spectrum of α-quartz. The value of F_1 attributed to Scott *et al.*[20] was calculated by this author using Eq. (4) and their spectral data. Gaskell *et al.*[21,22] arrived at their value[23] using a form of Eq. (12), the necessary $\epsilon''(\nu)$ spectrum being generated from a Kramers-Kronig analysis of their reflection spectrum for fused quartz. The value of F_1 given for Denisov *et al.*[3] was calculated by this author using Eq. (4) and their spectral data. The value listed for Galeener *et al.*[2] was calculated by this author using Eq. (4) and values of LO and TO frequencies obtained from peaks in their dielectric-loss spectra $\mathrm{Im}[-\epsilon^{-1}(\nu)]$ and $\mathrm{Im}\epsilon(\nu)$, respectively. The value of F_1 associated with Pliskin *et al.*[24] was found by this author using Eq. (16) for the main 1065-cm^{-1} optical-absorption peak of their thin a-SiO_2 film shown plotted in their paper.[25] Naiman *et al.*[13] obtained their value for F_1 by fitting a form of Eq. (5) to the AS_1 TO mode in the 1065-cm^{-1} region of a transmission spectrum of their thin oxide film.

Numerically, the values of F_1 shown in Table I cluster into three groups. The Spitzer and the Scott α-quartz and the Gaskell fused-quartz values are in reasonable agreement with each other despite the diversity of material forms and methods for finding F_1. Together they form the first group. Scott's value for α-quartz is somewhat higher than Spitzer's because of the failure of the Scott Raman spectrum to resolve the slight LO-TO splitting (2 or 3 cm^{-1}) of the AS_2 quartz E mode at 1162 cm^{-1}.

The Denisov and the Galeener F_1's for fused quartz form a second group whose values are significantly higher than those of the Spitzer group. Both values were obtained from a form of Eq. (4) using LO and TO spectral data. These anomalously high values suggest a failure, analogous to Scott's, to resolve an optically weak AS_2-mode LO-TO pair whose frequencies lie in the range between the AS_1-mode LO-TO-pair frequencies and whose LO-TO frequency splitting is significantly larger than the 2 or 3 cm^{-1} associated with the high Scott quartz value of F_1.

Pliskin's value and Naiman's value of F_1 for thin silica films comprise the third group. Although significantly smaller numerically than the bulk values of the Spitzer group, the methods by which these values for F_1 were obtained assure that they are correct for a-SiO_2 films.

TABLE I. Comparison of density-scaled mode strengths F_1 associated with the 1076-cm^{-1} AS_1 TO absorption mode of various forms of SiO_2 as reported in the literature or calculated from data reported therein. Units are cm^{-1} for ν_{L1} and ν_{T1}, the LO and TO frequencies of the AS_1 vibrational mode, respectively, and cm^{-2} for F_1. Units for the density η are g/cm^3.

	Spitzer *et al.* (Ref. 14)	Scott *et al.* (Ref. 20)	Gaskell *et al.* (Ref. 21)	Denisov *et al.* (Ref. 3)	Galeener *et al.* (Ref. 2)	Pliskin *et al.* (Ref. 24)	Naiman *et al.* (Ref. 13)
Material form:	α-quartz	α-quartz	Fused quartz	Fused quartz	Fused quartz	Thin[a] film	Thin[a] film
Spectral method:	Reflection (E mode)	Raman (E mode)	Reflection	Hyper-Raman	Reflection	Transmission	Transmission
ϵ_∞	2.356	2.356	2.11	2.11	2.11	2.14	2.14
ν_{L1}		1235		1255	1260		
ν_{T1}	1072	1072	1076.3	1065	1065	1065	1065
η	2.65[b]	2.65[b]	2.20[b]	2.20[b]	2.20[b]	2.24[c]	2.24[c]
F_1[d]	61 300	63 100	61 000	78 500	81 500	50 200	52 000

[a]1000 °C oxides thermally grown on silicon wafers.
[b]H. R. Phillip, Solid State Commun. **4**, 73 (1966).
[c]E. H. Nicollian and J. R. Brews, *MOS (Metal Oxide Semiconductor) Physics and Technology* (Wiley, New York, 1982), Table 14.3, p. 741.
[d]All values linearly scaled to the density of α-quartz.

Interestingly, the Gaskell bulk a-SiO_2 value for F_1 includes a contribution from the region of the high-frequency shoulder near 1200 cm^{-1} which constitutes approximately 15% of that value. By this author's estimate then, about 85% of the overall mode strength, or $\approx$51 850 cm^{-2}, resides in the 1076-cm^{-1} AS_1 TO absorption band, in reasonable agreement with the Pliskin and the Naiman a-SiO_2 film values for F_1.

This paper demonstrates that one way to account for the differences in the oscillator strengths of these three groups in a self-consistent manner is to assume mode coupling.[26] Disorder-induced coupling[21,22] between the AS_1 mode and the optically weak AS_2 mode in going from crystalline α-quartz to a-SiO_2 can give rise to increased LO-TO splitting of the AS_2 mode and, thereby, explain the anomalously high F_1 values attributed to Denisov and to Galeener in Table I. In addition, this disorder-induced coupling can bring about a reduction in TO strength of the AS_1 mode and, as a result, account for the low F_1 values attributed to Pliskin and to Naiman shown in Table I. The sum of the AS_1 and AS_2 TO-mode strengths for a-SiO_2 can then yield a value in agreement with the Spitzer value for F_1 and, at the same time, explain the 85–15 % apportionment of the Gaskell F_1 value described above.

III. MODE COUPLING

In this section the necessary mathematics is developed which will be applied in Sec. V to the specific case of coupling between the AS_1 and AS_2 modes in a-SiO_2. The objective here is to obtain analytic expressions for the imaginary part of the dielectric response of a material with two coupled modes to an external field from which the mode strengths and the LO and TO frequencies of the coupled modes can be determined.

The analysis begins, in Sec. III A, with a description of the equations of motion of two linearly coupled electric-dipole oscillators driven by an electric field which are used to model the coupled optical modes. Next, the equation expressing the polarization of the coupled oscillators in terms of the dipole moments of the oscillators is introduced to complete the coupled-mode model. In Sec. III B, the effects of geometric depolarization are considered that lead to a splitting of each of the mechanically coupled oscillator modes into a LO and a TO mode. Then, two separate complex dielectric response functions are defined and determined, one of which expresses the TO response of the dielectric model to an external electromagnetic radiation field and, the other, the LO response to an external electromagnetic radiation field. In Sec. III C, separate expressions for the imaginary parts of both the LO and TO dielectric response functions are derived in order to obtain equations expressing both the LO and TO strengths and the LO and TO vibrational frequencies of the coupled-mode model. In order to make these latter equations as tractable as possible, the imaginary parts of the dielectric response functions are derived in the limit of zero damping. (This procedure is considered valid because the frequency broadening of a single oscillator due to damping is small compared to the distribution of oscillator frequencies of a single vibrational mode in an amorphous material.) Then the strengths and frequencies of the coupled system are described and shown to be mixtures of the original strengths and frequencies of the uncoupled system. Finally, in Sec. III D, the relations between LO and TO frequency levels of the coupled system and, in particular, the interspersion principle of LO and TO modes alternating with each other in frequency are described.

A. Coupled classical oscillators

The dielectric response of materials with coupled optic vibrational modes can usually be analyzed in terms of a

system of linearly coupled classical electric-dipole oscillators independent of whether the coupling arises from harmonic or anharmonic interactions. By requiring harmonic solutions $\sim\exp(-i\omega t)$, and letting $\omega=2\pi c\nu$, where c is the velocity of light and ν is the wave number, the classical equations of motion for a material with two linearly coupled optical modes can be expressed in the form[26]

$$(\nu_{T11}^2-i\nu\gamma_{11}-\nu^2)X_1+(\nu_{T12}^2-i\nu\gamma_{12})X_2=Q_1E^{int}\ ,$$
$$(\nu_{T12}^2-i\nu\gamma_{12})X_1+(\nu_{T22}^2-i\nu\gamma_{22}-\nu^2)X_2=Q_2E^{int}\ , \tag{17}$$

where $X_{1,2}$ and $Q_{1,2}$ are reduced forms of the coupled-optic-mode vibrational amplitudes x_1,x_2 and transverse effective charges e_{T1}^*,e_{T2}^*, respectively, defined by the relations

$$X_j=2\pi c(\bar{M}_j/\Omega)^{1/2}x_j,\quad j=1,2 \tag{18}$$

and

$$Q_j=e_{Tj}^*/2\pi c(\bar{M}_j\Omega)^{1/2},\quad j=1,2 \tag{19}$$

$\bar{M}_1$ and $\bar{M}_2$ are the reduced masses of the coupled-optic-mode oscillators, and Ω is the volume of the material's unit cell. Other parameters in Eq. (17) are the unperturbed transverse oscillator frequencies ν_{T11} and ν_{T22}, their respective damping coefficients γ_{11} and γ_{22}, and the transverse mechanical coupling terms expressed as an interaction frequency ν_{T12} and an interaction-damping coefficient γ_{12}. The quantity E^{int} in Eq. (17) is the macroscopic electric field inside the material; corrections due to effects of the local field are already included in the transverse parameters e_{T1}^*, e_{T2}^*, ν_{T11}, ν_{T22}, and ν_{T12}. Restrictions on the parameters are those of a passive linear realizable system; ν_{T11}^2, ν_{T22}^2, γ_{11}, and γ_{22} must be positive, $\nu_{T11}^2\nu_{T22}^2$ must be greater than ν_{T12}^4, and $\gamma_{11}\gamma_{22}$ must be greater than γ_{12}^2.

The polarization of the material P is given by

$$P=\frac{\epsilon_\infty-1}{4\pi}E^{int}+Q_1X_1+Q_2X_2\ . \tag{20}$$

In Eq. (20) the first term represents the electronic polarization of the material. The remaining terms represent the polarization due to the per-unit-volume dipole moments of the coupled oscillators. By restricting the analysis to cases in which the polarization and electric field vectors are parallel (an appropriate assumption for an amorphous material), they can be treated as scalars, allowing Eqs. (17) and (20) to be written in scalar form.

Expressed in matrix form, the equations of motion given by Eq. (17) become

$$G_TX=QE^{int}\ , \tag{21}$$

where

$$G_T=\begin{bmatrix}\nu_{T11}^2-i\nu\gamma_{11}-\nu^2 & \nu_{T12}^2-i\nu\gamma_{12}\\ \nu_{T12}^2-i\nu\gamma_{12} & \nu_{T22}^2-i\nu\gamma_{22}-\nu^2\end{bmatrix},$$
$$X=\begin{bmatrix}X_1\\X_2\end{bmatrix},\quad Q=\begin{bmatrix}Q_1\\Q_2\end{bmatrix}. \tag{22}$$

Similarly, when expressed in matrix notation, the scalar equation for the material polarization, P, given by Eq. (20) becomes

$$P=\frac{\epsilon_\infty-1}{4\pi}E^{int}+\tilde{Q}X\ , \tag{23}$$

where $\tilde{Q}$ is the transpose of the column vector Q.

B. Dielectric response function

Of interest in this paper is the dielectric response function ϵ^r which represents the dielectric response of the coupled-mode material to the *external* electric field of the incident radiation E^{ext}. Introduced by Burstein *et al.*,[27] ϵ^r is defined by the relation

$$\epsilon^rE^{ext}=E^{ext}+4\pi P\ . \tag{24}$$

As will be shown, this response function ϵ^r is of interest because it allows the LO and TO responses of a dielectric material to external electromagnetic radiation to be expressed as separate functions from which, respectively, both the LO- and TO-mode strengths and vibrational frequencies can be calculated.

In order to express ϵ^r in terms of the coupled-mode parameters discussed in Sec. III A, the relationship between E^{ext} and E^{int} needs to be established. For plane-wave solutions of $E^{int}\sim\exp(i\mathbf{q}\cdot\mathbf{r})$, where $\mathbf{q}$ is the wave vector in the material, E^{ext} is related to E^{int} by[27]

$$E^{int}=E^{ext}-LP\ , \tag{25}$$

where L is a geometric depolarization factor arising from a property of the electromagnetic field equations in bulk material that the displacement field $D=E^{int}+4\pi P$ must vanish in the direction of $\mathbf{q}$. Thus, for a bulk material or for a slab of dielectric material of sufficient thickness d that $|\mathbf{q}|d\gg1$, L is given by

$$L=\begin{cases}0 & \text{for } \mathbf{E}^{int}\perp\mathbf{q}\ ,\\ 4\pi & \text{for } \mathbf{E}^{int}\parallel\mathbf{q}\ .\end{cases} \tag{26a}$$

In the case of the very thin slab or film of dielectric material with which this paper is concerned, such that $|\mathbf{q}|d\ll1$, the presence of electric-field-induced surface charges on the slab faces requires that D vanish in the direction normal to the slab faces rather than the direction of $\mathbf{q}$. Thus, for a sufficiently thin slab, L is determined by the geometry of the material and is given by

$$L=\begin{cases}0 & \text{for } \mathbf{E}^{int} \text{ parallel to the slab plane}\ ,\\ 4\pi & \text{for } \mathbf{E}_{int} \text{ perpendicular to the slab plane}\ .\end{cases} \tag{26b}$$

As a result of the fact that L can take on two different values in a dielectric material, the system of electric-dipole oscillators representing the dielectric can exhibit two different vibrational modes: a transverse mode ($\mathbf{E}^{int}\perp\mathbf{q}$) corresponding to $L=0$, and a longitudinal mode ($\mathbf{E}^{int}\parallel\mathbf{q}$) corresponding to $L=4\pi$. Thus, upon eliminating E^{int} and P from among Eqs. (21)–(26), the equations of motion and dielectric response can be expressed in the following manner:

For $L=0$,

$$G_T X_T = Q E^{\text{ext}}$$

and (27)

$$\epsilon_T^r E^{\text{ext}} = \epsilon_\infty E^{\text{ext}} + 4\pi \tilde{Q} X_T \ ,$$

where G_T is the transverse dynamic matrix given by Eq. (22), X_T is the transverse vibrational amplitude matrix, and ϵ_T^r is the transverse dielectric response function.

For $L = 4\pi$

$$G_L X_L = \frac{1}{\epsilon_\infty} Q E^{\text{ext}}$$

and (28)

$$\epsilon_L^r E^{\text{ext}} = 2 - \frac{1}{\epsilon_\infty} + \frac{4\pi}{\epsilon_\infty} \tilde{Q} X_L \ .$$

where $G_L = G_T + 4\pi Q \tilde{Q} / \epsilon_\infty$ is the longitudinal dynamic vibrational matrix, X_L is the longitudinal vibrational amplitude matrix, and ϵ_L^r is the longitudinal dielectric response function.

In more explicit form, G_L is given by

$$G_L = \begin{bmatrix} \nu_{L11}^2 - i\nu\gamma_{11} - \nu^2 & \nu_{L12}^2 - i\nu\gamma_{12} \\ \nu_{L12}^2 - i\nu\gamma_{12} & \nu_{L22}^2 - i\nu\gamma_{22} - \nu^2 \end{bmatrix} , \quad (29)$$

where

$$\left.\begin{aligned} \nu_{Ljk}^2 &= \nu_{Tjk}^2 + \frac{4\pi}{\epsilon_\infty} Q_j Q_k \\ \nu_{Ljk}^2 &= \nu_{Lkj}^2, \quad \nu_{Tjk}^2 = \nu_{Tkj}^2 \end{aligned}\right\} \ j = 1,2, \quad k = 1,2 \ . \quad (30)$$

As a result of having separated the dielectric response function into its transverse and longitudinal forms, the only expressions relating the longitudinal and transverse coupled-mode parameters are now those given by Eq. (30).

Explicit expressions for ϵ_T^r and ϵ_L^r can be written directly from an inspection of Eq. (27) and Eq. (28), respectively. Thus, from Eq. (27), it is seen that

$$\epsilon_T^r = \epsilon_\infty + 4\pi \tilde{Q} G_T^{-1} Q \ , \quad (31)$$

and from Eq. (28) that

$$\epsilon_L^r = 2 - \frac{1}{\epsilon_\infty} + \frac{4\pi}{\epsilon_\infty^2} \tilde{Q} G_L^{-1} Q \ . \quad (32)$$

Relationships between ϵ_T^r and ϵ_L^r and the material dielectric function ϵ, where ϵ is defined in terms of E^{int} by the equation

$$\epsilon E^{\text{int}} = E^{\text{int}} + 4\pi P \ ,$$

can be found by comparing this equation with Eq. (24), making use of Eq. (25) in the process. The relations which obtain are

$$\epsilon_T^r = \epsilon$$

and (33)

$$\epsilon_L^r = 2 - \epsilon^{-1} \ ,$$

where the equivalence between ϵ_T^r and ϵ occurs because in the transverse ($L = 0$) case E^{int} and E^{ext} are equal. By making use of Eqs. (22), (29), and (30), ϵ_T^r and ϵ_L^r as given by Eqs. (31) and (32), respectively, can be expressed as explicit functions of ν of the forms

$$\epsilon_T^r(\nu) = \epsilon_\infty + 4\pi \frac{(\nu_{T22}^2 - i\nu\gamma_{22} - \nu^2)Q_1^2 - 2(\nu_{T12}^2 - i\nu\gamma_{12})Q_1 Q_2 + (\nu_{T11}^2 - i\nu\gamma_{11} - \nu^2)Q_2^2}{(\nu_{T11}^2 - i\nu\gamma_{11} - \nu^2)(\nu_{T22}^2 - i\nu\gamma_{22} - \nu^2) - (\nu_{T12}^2 - i\nu\gamma_{12})^2} \quad (34)$$

and

$$\epsilon_L^r(\nu) = 2 - \frac{1}{\epsilon_\infty} + 4\pi \frac{(\nu_{L22}^2 - i\nu\gamma_{22} - \nu^2)Q_1^2 - 2(\nu_{L12}^2 - i\nu\gamma_{12})Q_1 Q_2 + (\nu_{L11}^2 - i\nu\gamma_{11} - \nu^2)Q_2^2}{(\nu_{L11}^2 - i\nu\gamma_{11} - \nu^2)(\nu_{L22}^2 - i\nu\gamma_{22} - \nu^2) - (\nu_{L12}^2 - i\nu\gamma_{12})^2} \ , \quad (35)$$

where, for $j = 1,2$ and $k = 1,2$, the longitudinal levels ν_{Ljk}^2 are defined by Eq. (30).

C. Dielectric-loss response-function model

In general, ϵ_T^r and ϵ_L^r are complex. Of particular interest are the loss or imaginary parts of these dielectric response functions $\epsilon_T^{r\prime\prime}$ and $\epsilon_L^{r\prime\prime}$ since they are related both to mode strength in dielectric materials through Eq. (12) and to absorption in thin dielectric films through Eqs. (14) and (15). The defining relations

$$\left.\begin{aligned} 2i\epsilon_T^{r\prime\prime} &= \epsilon_T^r - \epsilon_T^{r*} \ , \\ 2i\epsilon_L^{r\prime\prime} &= \epsilon_L^r - \epsilon_L^{r*} \end{aligned}\right. \quad (36)$$

can be used, respectively, to obtain $\epsilon_T^{r\prime\prime}$ from Eq. (34) and $\epsilon_L^{r\prime\prime}$ from Eq. (35). Usually, the resulting expressions for $\epsilon_T^{r\prime\prime}$ and $\epsilon_L^{r\prime\prime}$ are found not to fit the experimental spectral data of amorphous dielectrics. The difficulty arises because each of the various vibrational modes of an amorphous material really should be represented by an essentially continuous Gaussian-like frequency distribution of Lorentzian oscillators with little or no damping rather than a single, highly damped Lorentzian.[11–13] Accordingly, the procedure to be used in this paper for obtaining $\epsilon_T^{r\prime\prime}$ and $\epsilon_L^{r\prime\prime}$ from Eqs. (34) and (35), respectively, is to calculate these quantities in the limit of zero damping. In view of the fact that Lorentzian widths obtained from crystalline quartz data are ≈ 7 cm^{-1},[14,21] while the

Gaussian widths found from a-SiO_2 data are ≈ 70 cm^{-1},[13,21] this approach appears plausible. When necessary, suitable forms of these calculated quantities can be arbitrarily broadened by convoluting them with a Gaussian-frequency density distribution of the form

$$g(\nu')=(2\pi\sigma^2)^{-1/2}\exp(-\nu'^2/2\sigma^2) .$$

Thus, from Eqs. (34) and (36), in the limit as γ_{11}, γ_{22}, and $\gamma_{12}\to 0$ such that $\gamma_{11}\gamma_{22}>\gamma_{12}^2$, it can be shown that

$$\begin{aligned}\nu\epsilon_T''(\nu)\to 2\pi^2\{&[\pm(1-\Lambda_T^2)^{1/2}Q_1-(\Lambda_T^2)^{1/2}Q_2]^2[\delta(\nu-\bar\nu_{T1})+\delta(\nu+\bar\nu_{T1})]\\&+[(\Lambda_T^2)^{1/2}Q_1\pm(1-\Lambda_T^2)^{1/2}Q_2]^2[\delta(\nu-\bar\nu_{T2})+\delta(\nu+\bar\nu_{T2})]\} ,\end{aligned} \tag{37}$$

where, in Eq. (37), the " + " sign holds for $\nu_{T12}^2>0$ and the "−" sign for $\nu_{T12}^2<0$, $\delta(\xi)$ is the Dirac δ function, $\pm\bar\nu_{T1}$ and $\pm\bar\nu_{T2}$ are the zeros of

$$[(\nu_{T11}^2-\nu^2)(\nu_{T22}^2-\nu^2)-(\nu_{T12}^2)^2] ,$$

and Λ_T^2 is a transverse coupling coefficient given by

$$\Lambda_T^2=\Gamma_T^2/(\Delta_T^2+2\Gamma_T^2) \tag{38}$$

such that, for $\nu_{T11}^2<\nu_{T22}^2$,

$$\begin{aligned}&\Gamma_T^2=\nu_{T11}^2-\bar\nu_{T1}^2=\bar\nu_{T2}^2-\nu_{T22}^2 ,\\&2\Gamma_T^2=[(\Delta_T^2)^2+(2\nu_{T12}^2)^2]^{1/2}-\Delta_T^2 ,\end{aligned} \tag{39}$$

and

$$\Delta_T^2=\nu_{T22}^2-\nu_{T11}^2 .$$

Figure 2 illustrates the effect of transverse-mode coupling on the transverse-mode frequencies in the limit of zero damping. It can be seen from Eqs. (37)–(39) that, in the zero-damping limit, the transverse dielectric-loss response function $\nu\epsilon_T''$ exhibits two Dirac δ-function peaks as a function of ν^2: one at $\bar\nu_{T1}^2$ and the other at $\bar\nu_{T2}^2$, shifted apart in magnitude from their respective uncoupled levels ν_{T11}^2 and ν_{T22}^2 by Γ_T^2. For finite values of the quantity ν_{T12}^2, which characterizes the actual coupling between the two transverse modes, Γ_T^2 is always finite and greater than zero; it vanishes if and only if ν_{T12}^2 vanishes.

Equation (37) shows the effect of the coupling on reduced transverse effective dipolar charge associated with the coupled oscillator modes. For the coupled absorption level $\bar\nu_{T1}^2$, the reduced charge is $(1-\Lambda_T^2)^{1/2}Q_1-\Lambda_T Q_2$ and, for $\bar\nu_{T2}^2$, it is $\Lambda_T Q_1+(1-\Lambda_T^2)^{1/2}Q_2$, where Λ_T^2 is the transverse coupling coefficient defined by Eq. (38). Λ_T^2 vanishes when Γ_T^2 and hence ν_{T12}^2 vanishes. In this case, the reduced charges and mode levels take on their uncoupled values of Q_1,ν_{T11}^2 and Q_2,ν_{T22}^2. As Λ_T^2 increases, the values of the reduced charges associated with $\bar\nu_{T1}^2$ and $\bar\nu_{T2}^2$ change, with one increasing in magnitude and the other decreasing. Which is which depends on the signs of Q_1 and Q_2. The sum of the squares of the reduced charges is invariant to changes in Λ_T^2 and is equal to the quantity $Q_1^2+Q_2^2$.

Since $\epsilon_T'=\epsilon$ from Eq. (33) and therefore $\nu\epsilon_T''=\nu\epsilon''$, it can be shown from Eqs. (11), (12), and (37) that the sum F of the oscillator strengths F_1 and F_2 for the coupled modes is equal to the sum of the squares of the reduced charges. Accordingly, $F=F_1+F_2=Q_1^2+Q_2^2$ is independent of the mode-coupling strength, at least in the limit of no damping.

Similarly, from Eqs. (35) and (36), and again in the limit as γ_{11}, γ_{22}, and $\gamma_{12}\to 0$ such that $\gamma_{11}\gamma_{22}>\gamma_{12}^2$, it can be shown that

$$\begin{aligned}\nu\epsilon_L''(\nu)\to 2\pi^2\{&[\pm(1-\Lambda_L^2)^{1/2}Q_1-(\Lambda_L^2)^{1/2}Q_2]^2[\delta(\nu-\bar\nu_{L1})+\delta(\nu+\bar\nu_{L1})]\\&+[(\Lambda_L^2)^{1/2}Q_1\pm(1-\Lambda_L^2)^{1/2}Q_2]^2[\delta(\nu-\bar\nu_{L2})+\delta(\nu+\bar\nu_{L2})]\} ,\end{aligned} \tag{40}$$

where, in Eq. (40), the " + " sign holds for $\nu_{L12}^2>0$ and the "−" sign for $\nu_{L12}^2<0$, $\delta(\xi)$ is again the Dirac δ function, $\pm\bar\nu_{L1}$ and $\pm\bar\nu_{L2}$ are the zeros of

$$[(\nu_{L11}^2-\nu^2)(\nu_{L22}^2-\nu^2)-(\nu_{L12}^2)^2] ,$$

and Λ_L^2 is a longitudinal coupling coefficient given by

$$\Lambda_L^2=\Gamma_L^2/(\Delta_L^2+2\Gamma_L^2) \tag{41}$$

such that, for $\nu_{L11}^2<\nu_{L22}^2$,

$$\begin{aligned}&\Gamma_L^2=\nu_{L11}^2-\bar\nu_{L1}^2=\bar\nu_{L2}^2-\nu_{L22}^2 ,\\&2\Gamma_L^2=[(\Delta_L^2)^2+(2\nu_{L12}^2)^2]^{1/2}-\Delta_L^2 ,\end{aligned} \tag{42}$$

and

$$\Delta_L^2=\nu_{L22}^2-\nu_{L11}^2 .$$

For the case in which $\nu_{L11}^2 > \nu_{L22}^2$, the numerical subscripts in Eqs. (40)–(42) must be interchanged, i.e., let $1 \rightarrow 2$ and $2 \rightarrow 1$.

Figure 3 illustrates the effect of longitudinal mode coupling on the longitudinal mode frequencies in the limit of zero damping. As in the transverse case, it can be seen from Eqs. (40)–(42) that, in the zero-damping limit, the longitudinal dielectric-loss response function $\nu\epsilon_L''$ exhibits its two Dirac δ-function peaks as a function of ν^2: one at $\bar{\nu}_{L1}^2$ and the other at $\bar{\nu}_{L2}^2$, shifted apart in magnitude from their respective uncoupled levels ν_{L11}^2 and ν_{L22}^2 by Γ_L^2. For finite values of the quantity ν_{L12}^2, which characterizes the actual coupling between the two longitudinal modes, Γ_L^2 is always finite and greater than zero; it vanishes if and only if ν_{L12}^2 vanishes.

Equation (40) shows the effect of coupling on reduced effective dipolar charge associated with the coupled longitudinal oscillator modes. For the coupled longitudinal absorption level $\bar{\nu}_{L1}^2$, the reduced charge is $(1-\Lambda_L^2)^{1/2}Q_1 - \Lambda_L Q_2$ and, for $\bar{\nu}_{L2}^2$, it is $\Lambda_L Q_1 + (1-\Lambda_L^2)^{1/2}Q_2$, where Λ_L^2 is the longitudinal coupling coefficient defined by Eq. (41). Λ_L^2 vanishes when Γ_L^2 and hence ν_{L12}^2 vanishes. In this case, the reduced charges and mode levels take on their uncoupled values of Q_1, ν_{L11}^2 and Q_2, ν_{L22}^2. As Λ_L^2 increases, the values of the reduced charges associated with $\bar{\nu}_{L1}^2$ and $\bar{\nu}_{L2}^2$ change, with one increasing in magnitude and the other decreasing. Which is which depends on the signs of Q_1 and Q_2. The sum of the squares of the reduced charges is invariant to changes in Λ_L^2 and is equal to the quantity $Q_1^2 + Q_2^2$.

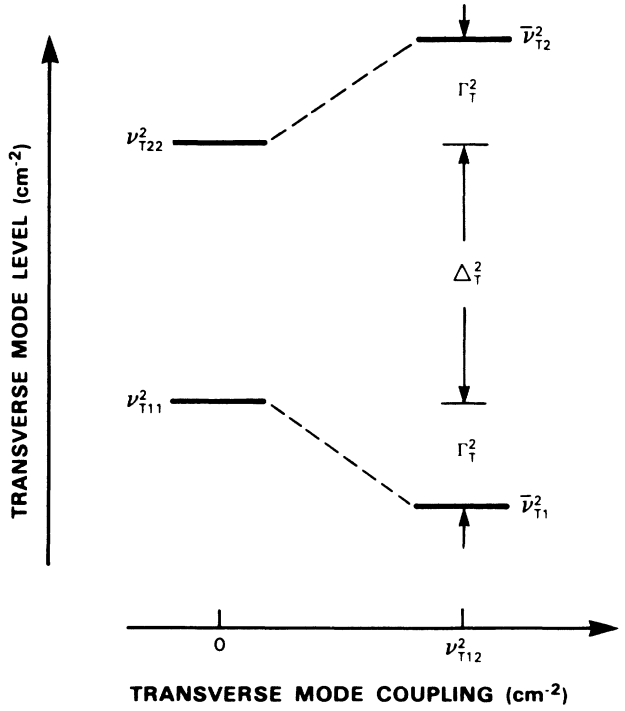

FIG. 2. Effect of increasing transverse mode coupling ν_{T12}^2 on the transverse mode levels $\bar{\nu}_{T1}^2$ and $\bar{\nu}_{T2}^2$.

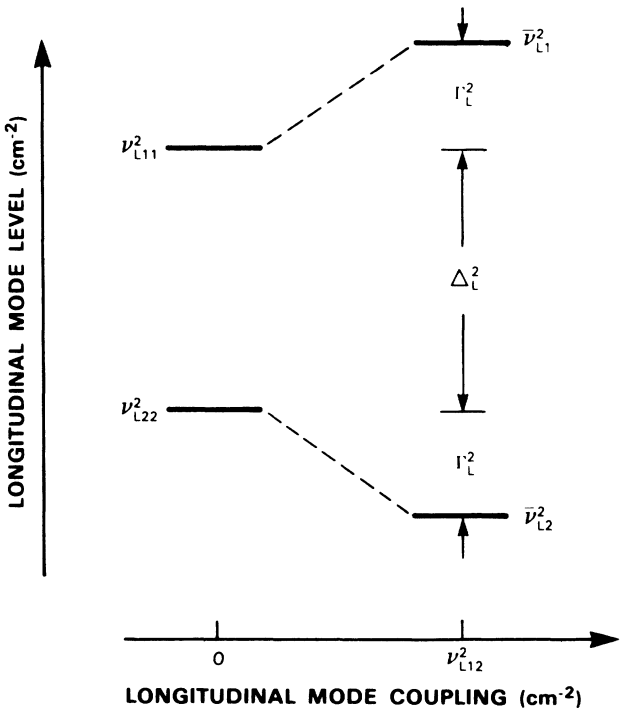

FIG. 3. Effect of increasing longitudinal mode coupling ν_{L12}^2 on the longitudinal mode levels $\bar{\nu}_{L1}^2$ and $\bar{\nu}_{L2}^2$.

D. Interspersion of LO- and TO-mode levels

It should be noted that the LO- and TO-mode levels shown, respectively, in Figs. 2 and 3 are not unrelated to each other, even in the absence of the transverse mechanical coupling parameter ν_{T12}^2. For $\nu_{T12}^2 = 0$, it can be seen from Eq. (30) that $\nu_{L12}^2 = 4\pi Q_1 Q_2 / \epsilon_\infty$. Thus, the longitudinal coupling parameter ν_{L12}^2 does not necessarily vanish when ν_{T12}^2 does, unless either Q_1 or Q_2 or both are zero. This type of coupling between the longitudinal modes exists independent of ν_{T12}^2 due to the interaction between dipolar vibrational modes through the polarization-induced internal field term, $-4\pi P$, of Eq. (25) found upon taking $L = 4\pi$ under the conditions indicated by Eq. (26). This polarization-induced field coupling of the dipole charge (charge coupling) acts in such a manner as to ensure that an LO-mode level is always interspersed between any two successive TO-mode levels.

Two cases of interspersion of LO and TO modes are of interest here. They are shown illustrated in Figs. 4(a) and 4(b). Each case involves two LO-TO-mode pairs for which there is no mechanical coupling between the modes, i.e., $\nu_{T12}^2 = 0$, and the higher-frequency TO mode is the T22 mode, i.e., $\nu_{T22}^2 > \nu_{T11}^2$. There are no restrictions as to the location of the uncoupled LO modes other than the normal one of lying higher in frequency than their respective TO mode.[28] In the first case, Fig. 4(a), the uncoupled L22 mode is taken to lie higher in frequency than the uncoupled L11 mode. In the second case, Fig. 4(b), the opposite is taken to be true, i.e., the uncoupled L22- and T22-mode–pair frequencies lie sandwiched

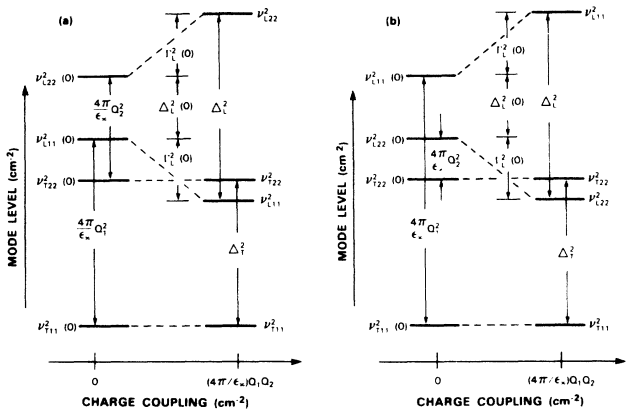

FIG. 4. Effect of charge coupling on the unperturbed ($\nu^2_{T12}=0$) longitudinal mode levels ν^2_{L22} and ν^2_{L11} (a) for $\nu^2_{L22}>\nu^2_{L11}$ and (b) for $\nu^2_{L11}>\nu^2_{L22}$.

between the uncoupled L11- and T11-mode–pair frequencies. Upon turning "on" the charge coupling between the two modes, the longitudinal levels "repel" each other, as shown in the figures each by an amount $\Gamma^2_L(0)$ from its uncoupled position. The quantity $\Gamma^2_L(0)$ is the magnitude of the longitudinal-mode level shift for $\nu^2_{T12}=0$. As illustrated in Figs. 4(a) and 4(b), and analytically in the Appendix, $\Gamma^2_L(0)$ is sufficiently large in each case to depress the lower lying of the two uncoupled LO modes below the level of the T22 mode. Figure 4(a) shows the usual situation that is observed when the charge coupling is taken into account, namely the LO and TO modes are properly interspersed and the LO modes lie higher in frequency than their respective TO modes. In Fig. 4(b) the situation shown with the charge coupling taken into account is somewhat different; the LO and TO modes are properly interspersed and the L11 mode lies higher in frequency than the T11 mode, but the L22-T22 frequency positions are reversed, with the T22 mode lying higher in frequency than the L22 mode. An examination of Fig. 4(b) shows that this comes about as a result of the uncoupled L22 mode lying lower in frequency than the L11 mode. Thus, for a LO-TO pair lying sandwiched between the frequencies of another LO-TO pair, interspersion is accommodated by inversion of the LO-TO-mode frequencies of the sandwiched pair.

IV. EXPERIMENT

A. Procedures

To test the theory of mode coupling in a-SiO_2, oxide films were prepared, characterized by ellipsometry, and their ir-absorption spectra obtained for both normally incident and obliquely incident light. Oxide films ranging in thickness from 10 to 100 nm were grown thermally on 3-in.-diam single-crystal (100)-oriented Si wafers. The Si wafers themselves were phosphorus-doped 1 Ω cm n type, 14–16 mils thick, and optically polished on both sides to facilitate the ir studies. Prior to oxidation the wafers were given a RCA-type peroxide cleaning including a HF dip, rinsed thoroughly in deionized water, and spun dry under a clean dry nitrogen blanket. After chemical treatment the wafers were put into the oxidation furnace by inserting them into 800 °C oxygen and ramped up to 1000 °C in 15 min. The wafers were oxidized on both sides in pure dry oxygen at 1000 °C for various lengths of time depending on the thickness desired. Oxidized wafers were removed from the furnace by a 15-min ramp-down in dry nitrogen to 800 °C, at which point they were pulled from the furnace. All ambient gases were at atmospheric pressure.

Ellipsometry was used to characterized the oxide films in terms of their thickness and optical index of refraction. A Rudolf Research model AutoEl automatic ellipsometer was used to take the ellipsometric data. This instrument generated Δ and Ψ readings from which calculations of the optical index and film thickness were made using the NBS ellipsometer program.[29] Readings were taken at a wavelength of 632.8 nm with a sensitivity of 0.04° in both Δ and Ψ. The optical index of the silicon substrate, n_{Si}, at this wavelength was taken to be $3.856(1+i0.0074)$.[13] Under these conditions, errors in the calculation of the index and thickness of the films were ±0.002 and ±0.1 nm, respectively.

All ir-absorption spectra were measured with an IBM FTIR-32 Fourier-transform infrared spectrophotometer. The spectral data were obtained from Si single-crystal wafers optically polished and oxidized on both sides, referenced against an empty-beam background for absolute transmission, and against a bare silicon wafer for extraction of the oxide absorption. All spectra were each the average of 1000 passes taken at a resolution of 2 cm^{-1}. Seven-point, three-pass Savitzky-Golay smoothing[30] was used to reduce to a negligible level the effect of a periodic fringe pattern (≈ 4 cm^{-1}) that arises from internal reflections in the silicon wafers.

Infrared transmission through the bare silicon reference wafer in frequency regions of low absorption were found to be within 0.2% of the theoretical value $2n_{Si}/(1+n^2_{Si})$ calculated using a silicon index $n_{Si}=3.418$.[31] While the major absorption in crystalline silicon takes place around a narrow peak at 607 cm^{-1}, a small but appreciably structured amount of absorption extends from this peak all the way up to 1500 cm^{-1}.[32] Because of the interest of this paper in the spectral region from about 900 to 1400 cm^{-1}, the absorption spectrum of single-crystal silicon was deleted from the absorption spectra of oxidized wafers by subtracting a proportional amount of the absorption spectrum of the bare silicon reference wafer sufficient to eliminate the silicon 607-cm^{-1} line together with its structured high-frequency tail from the oxidized-wafer spectra. Thereafter, only the spectral region from about 900 to 1400 cm^{-1} was considered.

Normal-incidence beam absorption spectra of the oxidized wafers were obtained using unpolarized light. Oblique-incidence oxidized-wafer absorption spectra were obtained using polarized light. Polarization of the incident light beam was effected using a PTR Optics wire-grid polarizer, 15×15 mm^2 with 1200 wires/mm.

An arbitrary oblique angle of incidence θ for the beam was accomplished by arranging for the normal to the surface of the oxidized wafer to be tilted by the angle θ with respect to the incident beam. At oblique angles of incidence, two unique polarizations of the incident beam can be distinguished, depending on how the plane of the oxidized wafer is tilted with respect to the polarization direction of the incident beam: one is the case in which the electric (E) field vector of the incident light lies in the plane of the oxidized wafer (s polarization). The other is the case in which the magnetic (H) field vector of the incident light lies in the plane of the oxidized wafer (p polarization). s-polarized oblique-incidence oxidized-wafer absorption spectra are the same as the oxidized-wafer absorption spectra obtained using normally incident unpolarized light. p-polarized oblique-incidence oxidized-wafer absorption spectra exhibit new absorption peaks in addition to the absorption peaks found in the s-polarized absorption spectra due to the Berreman effect[7-9] discussed briefly in Sec. I and in more detail in Sec. IV B.

B. Results

Absorption spectral data for a number of oxidized silicon wafers with different oxide thicknesses ranging from approximately 10 to 100 nm were obtained by FTIR spectroscopy using normally incident light. Typical of oxide absorption spectra in the (900–1400)-cm^{-1} frequency range is the spectrum shown in Fig. 5. This spectrum is from a silicon wafer with 37 nm of oxide thermally grown at 1000 °C on each side, from which the silicon absorption spectrum has been deleted by the method described above. The mode strength of the main TO absorption peak near 1076 cm^{-1} was estimated using Eq. (16) and doing the integration by the simple technique of assuming a Gaussian shape for the main peak and calculating the area under it from the absorption peak height and the full width at half the maximum peak height (FWHM). Comparison of this method of computing the TO-mode strength with the dispersion-analysis method used by Naiman[13] for his published transmission spectrum of a 36-nm-thick oxide (see Table I) produced agreement within 3%, both strengths having been scaled to the density of quartz. The scale factor used in this case was 2.65/2.24 ($\approx$1.18), where the density ratio of α-quartz to 1000 °C thermal oxide films on silicon was obtained from Table I.

Scaled TO-mode strengths for the 37-nm-thick oxide just described and for Naiman's 36-nm-thick oxide were found to be 50 700 and 52 000 cm^{-2}, respectively. These values are some 15–17 % below the 61 300-cm^{-2} value of crystalline quartz. Strictly speaking, for finite values of oxide thickness d, Eq. (16) calculates an apparent jth-mode strength F_j^* such that $F_j^* = F_j$ only in the limit as $d \to 0$. The complete equation relating F_j^* and F_j involves a functional dependence on d. In order to see if the calculated 1076-cm^{-1} TO-mode strengths of oxide films are dependent on d, as they should be, and to ascertain the correct value of that strength in the limit of vanishing d, values of 1076-cm^{-1} TO-mode strengths for oxide films of several different thicknesses are shown plotted as a function of d in Fig. 6. The null hypothesis that the calculated values of the 1076-cm^{-1} mode strength, F_1^*, for these films are independent of d results in a mean value for the mode strength $\bar{F}_1$ of 50 400 cm^{-2} plus or minus a standard deviation error of 1530 cm^{-2}. A fit of the data for F_1^* versus d to a straight line, shown plotted as a solid curve in Fig. 6, yields a significance level of 0.001 for (and hence rejects) the null hypothesis. Fits of F_1^* to second- and third-order polynomials with

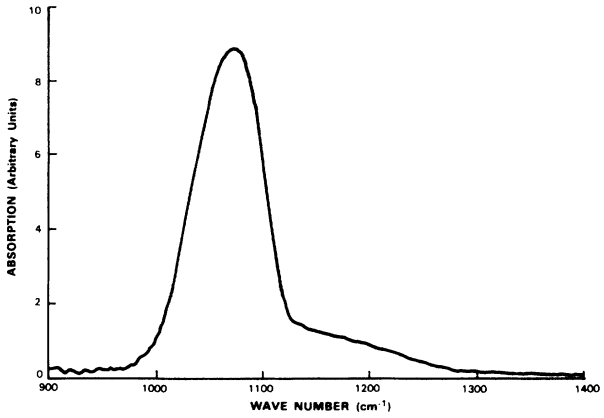

FIG. 5. Infrared TO absorption spectrum of two 37-nm-thick a-SiO_2 films one on each side of a (100) Si wafer in the region of the AS vibrational mode. The actual height of the main absorption peak near 1075 cm^{-1} is 0.281 and the full width of the absorption peak at half the maximum peak height is 76.1 cm^{-1}, from which the apparent integrated oscillator strength of the AS_1 mode F_1^* is estimated from Eq. (16) of the text to be 50 700 cm^{-2}.

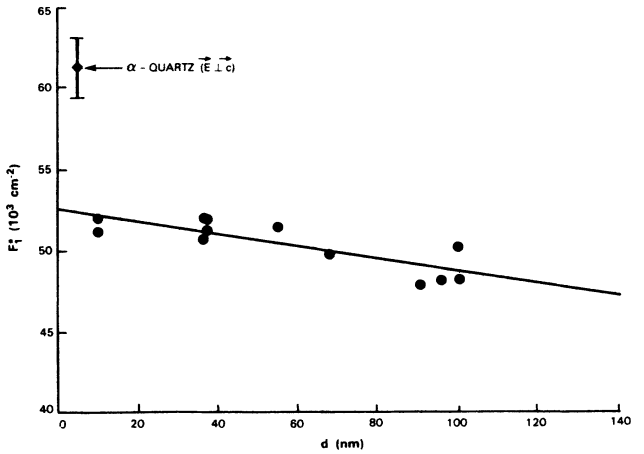

FIG. 6. Apparent 1075-cm^{-1} AS_1 TO-mode strength F_1^* of a-SiO_2 films grown thermally on (100) Si wafers vs film thickness d (solid circles). The solid line represents the best linear fit of the data. For comparison, the α-quartz 1072-cm^{-1} value for the AS_1 TO E-mode strength of 61 300±1800 cm^{-2} obtained by Spitzer *et al.* (Ref. 14) is shown on the graph (solid diamond with error bars).

significance levels of 0.003 and 0.005, respectively, are not as good as the first-order fit. Evaluated at $d=0$, the linear expression for F_1^* yields a density scaled value for $F_1=52\,530\pm520$ cm^{-2}. At roughly 85% of the value of F_1 for α-quartz (see Table I), this experimental value of F_1 for the 1076-cm^{-1} AS_1 TO-mode strength of a-SiO_2 represents significant difference in strength compared to the same mode in α-quartz.

In another set of experiments, oblique-incidence absorption spectral data of an oxidized silicon wafer with an oxide thickness of 100 nm were obtained with the FTIR equipment for various angles of incidence using p-polarized light. Shown in Fig. 7(a) is the absorption spectrum for the (900–1400)-cm^{-1} range of an oxide film for p-polarized light incident at 60° from normal. The broader of the two peaks located at approximately 1076 cm^{-1} is the AS_1 TO-mode absorption seen at normal incidence. The other peak in the figure at approximately 1256 cm^{-1} is due to absorption by the AS_1 LO vibrational mode which occurs as a consequence of the Berreman effect referred to earlier in this paper.[7–9]

Essentially, Berreman[9] showed that the transmission of oblique-incidence p-polarized light, T_p, through thin films to first order in $2\pi\nu d$ is given by[27]

$$T_p=1-\frac{2\pi\nu d}{\cos\theta}(\epsilon_T''\cos^2\theta+\epsilon_L''\sin^2\theta)\ , \tag{43}$$

where θ is the oblique incident angle. For sufficiently thin films, such that the second term in Eq. (43) is much less than unity, the absorption $\ln(I_{0p}/I_p)=\ln(1/T_p)$ can be approximated by the relation

$$\ln\left[\frac{I_{0p}}{I_p}\right]\approx\frac{2\pi\nu d}{\cos\theta}(\epsilon_T''\cos^2\theta+\epsilon_L''\sin^2\theta)\ . \tag{44}$$

For a silicon wafer supporting an identical oxide film on each of its sides, Eq. (44) must be modified to the relation

$$\ln\left[\frac{I'_{0p}}{I_p}\right]\approx\frac{2\pi d}{\cos\theta}\left[\frac{n_{Si}^2+3}{n_{Si}^2+1}\right](\nu\epsilon_T''\cos^2\theta+\nu\epsilon_L''\sin^2\theta)\ . \tag{45}$$

Equation (45) indicates that the absorption of p-polarized oblique incident light by the films is due to both LO and TO modes. This contrasts with the case of normally incident light in which absorption is due only to the TO modes as expressed for the jth TO mode by Eq. (15). In fact, in view of Eq. (33), when $\theta=0$ and considering only the jth-mode absorption, Eq. (45) reduces to Eq. (15).

It can be seen from Eq. (45) that p-polarized, oblique-incidence light absorption spectra of very thin films are proportional to the sum of their LO and TO absorptions scaled, respectively, by the absolute squares of the ratios of the incident-electric-field components normal and parallel to the plane of the films with respect to the total incident field. Such an oblique spectrum can be decomposed into its LO and TO component spectra by subtracting off the film's appropriately scaled normal incident TO absorption spectrum from its oblique absorption spectrum and thereby revealing the film's LO spectrum. This was done for the p-polarized, 60° oblique-incidence, 1000 °C thermal-oxide-film absorption spectrum shown in Fig. 7(a). The resulting LO and TO component absorption spectra for the thermally grown oxide films on silicon are shown in Figs. 7(b) and 7(c), respectively. In addition to the AS_1 LO and TO peaks at 1256 and 1076 cm^{-1}, respectively, both the LO and TO absorption spectra exhibit shoulders. These shoulders are more conspicuous in Figs. 8(a) and 8(b), where the respective LO and TO absorption spectra of Figs. 7(b) and 7(c) are shown as

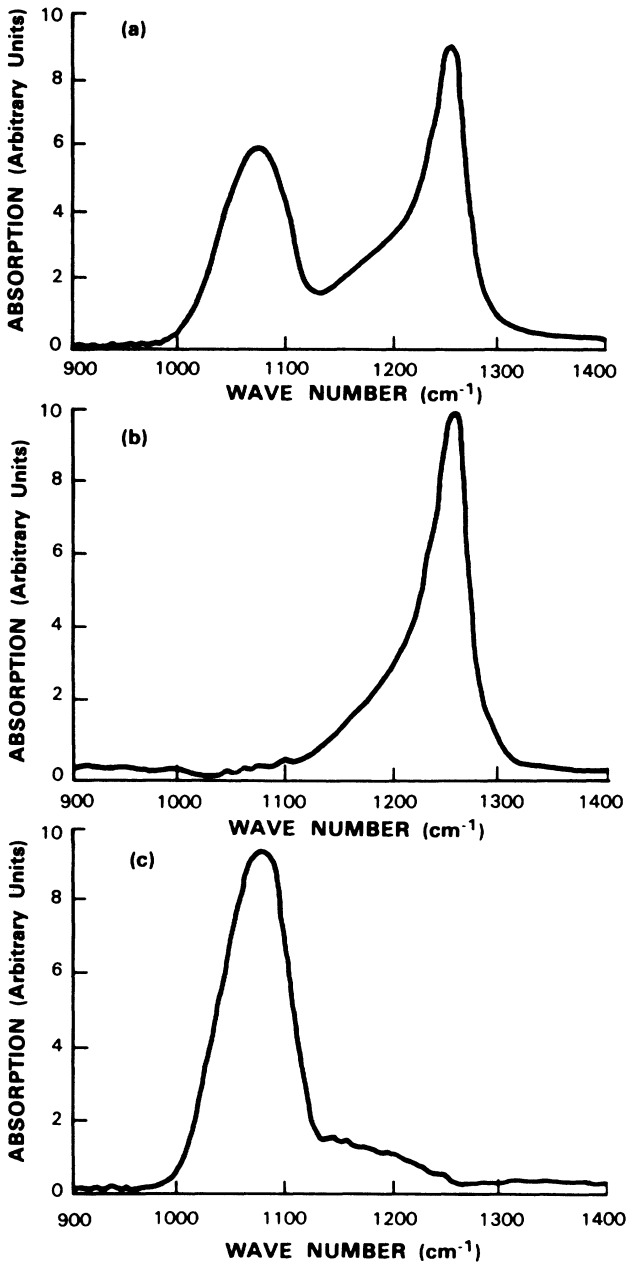

FIG. 7. (a) Oblique-incidence (60° from normal), p-polarized infrared-absorption spectrum in the region of the AS vibrational mode of identical a-SiO_2 films grown thermally on each side of a (100) Si wafer shown separated into its component (b) LO and (c) TO absorption spectra.

solid lines on semilogarithmic plots. The absorption-band centers responsible for these shoulders are estimated to be located at 1160 cm^{-1} in the case of the LO spectrum and at 1200 cm^{-1} in the case of the TO spectrum. Unfortunately, attempts to resolve these bands in a unique and systematic manner were frustrated by the dependence of the bands upon the choice of profiles for the main absorption bands at 1256 and 1076 cm^{-1}.

The high-frequency shoulder of the 1076-cm^{-1} TO absorption spectrum of a-SiO_2 as calculated from the reflectivity spectrum of vitreous silica has been analyzed by Gaskell and Johnson.[22] Their attempts to resolve the absorption band responsible for this shoulder also were frustrated by the dependence upon the choice of the profile for the 1076-cm^{-1} absorption peak. The presumption that some of the absorption in the high-frequency shoulder is attributable to absorption by the 1076-cm^{-1} mode in combination with other modes led Gaskell and Johnson to attempt to eliminate this absorption by adding a high-frequency tail to the 1076-cm^{-1} absorption profile. Their best estimate of the 1076-cm^{-1} high-frequency tail indicated a TO absorption peak in the high-frequency shoulder near 1200 cm^{-1}.

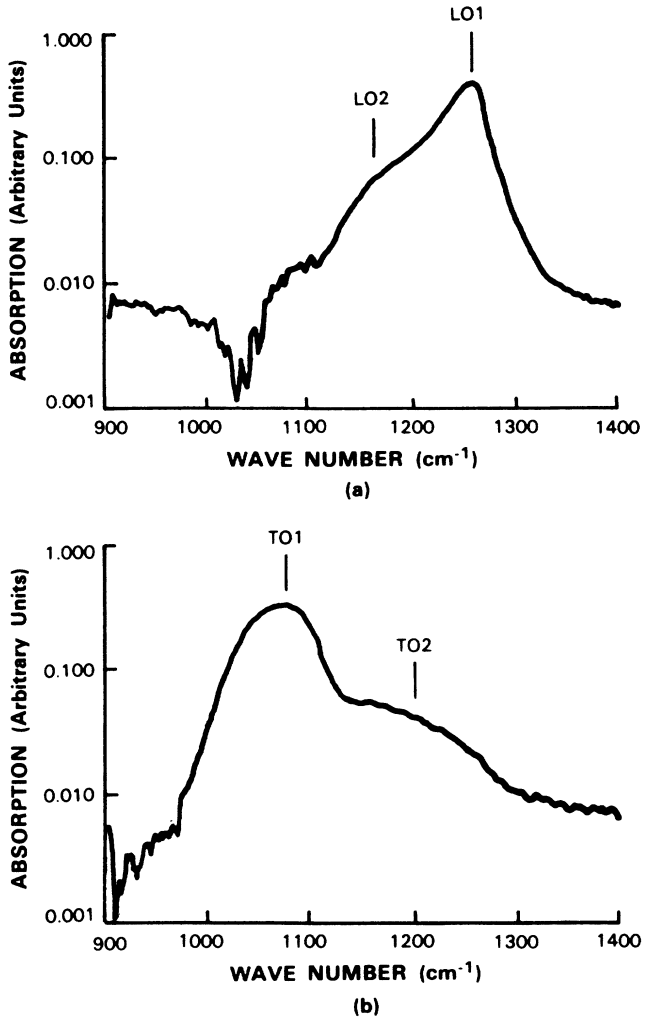

FIG. 8. Semilogarithmic intensity plots (to enhance the shoulders) of (a) the LO absorption spectrum of Fig. 7(b) with the approximate positions of the LO AS_1 (LO1) and the LO AS_2 (LO2) absorption peaks indicated by the vertical lines at 1256 and 1160 cm^{-1}, respectively, and (b) the TO absorption spectrum of Fig. 7(c) with the approximate positions of the TO AS_1 (TO1) and TO AS_2 (TO2) absorption peaks indicated by the vertical lines at 1076 and 1200 cm^{-1}, respectively.

Theoretical considerations led Gaskell and Johnson[22] to suggest that the 1076-cm^{-1} TO absorption is due to the AS_1 vibrational mode and that the TO absorption in the high-frequency shoulder with an absorption peak near 1200 cm^{-1} is due to the AS_2 mode. More recently, Lucovsky *et al.*[5] and Pai *et al.*[6] have suggested that, in a-SiO_2, the AS_2 mode is not only responsible for the infrared-absorption shoulder, but also gives rise to the Raman spectral peak observed by Galeener *et al.*[2] and, earlier, by Flubacher *et al.*[33] near 1200 cm^{-1}.

The LO intensity peak seen near 1256 cm^{-1} in the infrared spectrum for a-SiO_2 is absent in the Raman spectrum.[2,33] However, Denisov *et al.*,[3] using hyper-Raman spectroscopy, observed a strong peak at 1255 cm^{-1} that they conclude is the same mode as the 1260-cm^{-1} LO mode found by Galeener *et al.*[2] from an analysis of the infrared-reflection spectrum of fused quartz. At 1065 cm^{-1}, Denisov *et al.* observed the TO mode associated with their 1255-cm^{-1} LO mode. In addition, lying between this LO-TO pair at $\approx$1180 cm^{-1}, Denisov *et al.* observed another LO-TO pair that they were unable to resolve, but whose intensity peak they believed corresponds to the peak near 1200 cm^{-1} in the Raman spectrum of vitreous silica discussed above.

In summary, the experimental infrared, Raman, and hyper-Raman spectra of a-SiO_2 in the (900–1400)-cm^{-1} range appear to show two types of lattice-vibrational modes, each exhibiting some LO-TO frequency splitting. The most prominent vibrational mode, AS_1, exhibits a TO mode at a frequency of approximately 1076 cm^{-1} and a LO mode at a frequency of approximately 1256 cm^{-1}. Thin film measurements of the strength of this TO mode indicate a density-scaled value of F_1 equal to about 85% of that of the same mode in quartz. A second vibrational mode, AS_2, lying intermediate in frequency between the frequencies of the AS_1 LO-TO pair, exhibits a TO mode at $\approx$1200 cm^{-1} and a LO mode at $\approx$1160 cm^{-1}. Estimates of the density-scaled strength of the AS_2 TO mode, F_2, from bulk silica measurements indicate a value of F_2 equal to 3–5 times that of the same mode in quartz[22] or about 15% of the 1072-cm^{-1} mode in quartz. The most notable feature of these results is that, in going from α-quartz to a-SiO_2, the value of the sum of the AS TO density-scaled mode strengths, F_1+F_2, is approximately constant, increases in F_2 being at the expense of decreases in F_1.

Finally, it is important to note here that, altogether, there are four vibrational modes in a-SiO_2 which exhibit significant LO-TO level splitting.[3,17] Thus, in addition to the respective experimental values of 1256–1076 and 1160–1200 cm^{-1} for the coupled AS_1 and AS_2 LO-TO pairs obtained from Berreman-effect measurements as described above, the LO-TO frequencies of the two other

TABLE II. Comparison of experimental and estimated values of the a-SiO_2, density-scaled, 1076-cm^{-1} AS_1 TO-mode strength F_1 assuming four modes exhibit LO-TO splitting.

Oscillator mode j	$\bar{\nu}_{Lj}$ (cm^{-1})	$\bar{\nu}_{Tj}$ (cm^{-1})	$F_j^{(calc)}$ [a,b] (cm^{-2})	$F_j^{(meas)}$ [b] (cm^{-2})
1	1256	1076	≈51 840	52 530±520[c]
2	≈1160	≈1200	≈8740	
3	820	810		
4	507	457		

[a]Values estimated from Eqs. (52) and (53) of text with $\epsilon_\infty = 2.14$ and $N = 4$.
[b]Linearly scaled to the density of α-quartz (scale factor 2.650/2.237).
[c]Experimental value from Sec. IV B.

pairs will be needed for the analysis of the coupled-mode model. Experimental values of these two other pairs have been obtained by the author also from Berreman-effect measurements of thin a-SiO_2 films (not shown). One pair is at 820–810 cm^{-1} and is associated with the SS vibrational mode of the oxygen atoms. The other, at 507–457 cm^{-1}, is associated with the R vibrational mode of the oxygen atoms. The LO and TO frequencies of these four vibrational modes for a-SiO_2 are listed, respectively, in the columns of Table II labeled $\bar{\nu}_{Lj}$ and $\bar{\nu}_{Tj}$. Also listed in this table, in the column labeled $F_j^{(meas)}$, is the experimentally determined value for F_1 discussed earlier in this section.

V. ANALYSIS

Two vibrational modes whose systems become coupled as a result of some physical change in their environment, such that their individual mode strengths are altered but their sum is conserved, as in the case of the two AS vibrational modes of SiO_2 in going from α-quartz to a-SiO_2, are readily analyzed in terms of the coupled-mode model developed in Sec. III. Figure 9 shows the model of the AS coupled-mode vibrational levels involved in the analysis of a-SiO_2 together with the experimental values for these levels expressed in units of cm^{-2}. Analytic expressions for the coupled levels in terms of the model parameters Q_1, Q_2, Δ_T^2, and ν_{T12}^2 can be found from Eqs. (39) and (42) making appropriate use of Eqs. (30), (37), (38), (40), and (41). The resulting equations for the coupled levels can be used to construct the following analytical model for the coupled silica modes by taking the differences of the levels:

$$\frac{4\pi}{\epsilon_\infty}(Q_1^2+Q_2^2)=(\bar{\nu}_{L1}^2-\bar{\nu}_{T1}^2)+(\bar{\nu}_{L2}^2-\bar{\nu}_{T2}^2)\ , \tag{46}$$

$$\left[\frac{4\pi}{\epsilon_\infty}(Q_1^2-Q_2^2)-\Delta_T^2\right]^2+\left[2\nu_{T12}^2+2\frac{4\pi}{\epsilon_\infty}Q_1Q_2\right]^2 =(\bar{\nu}_{L1}^2-\bar{\nu}_{L2}^2)^2\ , \tag{47}$$

$$(\Delta_T^2)^2+(2\nu_{T12}^2)^2=(\bar{\nu}_{T2}^2-\bar{\nu}_{T1}^2)^2\ , \tag{48}$$

with the TO-mode strengths of the two coupled modes being given by

$$F_1=[\pm(1-\Lambda_T^2)^{1/2}Q_1-(\Lambda_T^2)^{1/2}Q_2]^2\ , \tag{49}$$

$$F_2=[(\Lambda_T^2)^{1/2}Q_1\pm(1-\Lambda_T^2)^{1/2}Q_2]^2\ , \tag{50}$$

where, in Eqs. (49) and (50), the "+" sign holds for $\nu_{T12}^2>0$ and the "−" sign for $\nu_{T12}^2<0$, and Λ_T^2 is related to ν_{T12}^2 by the equation

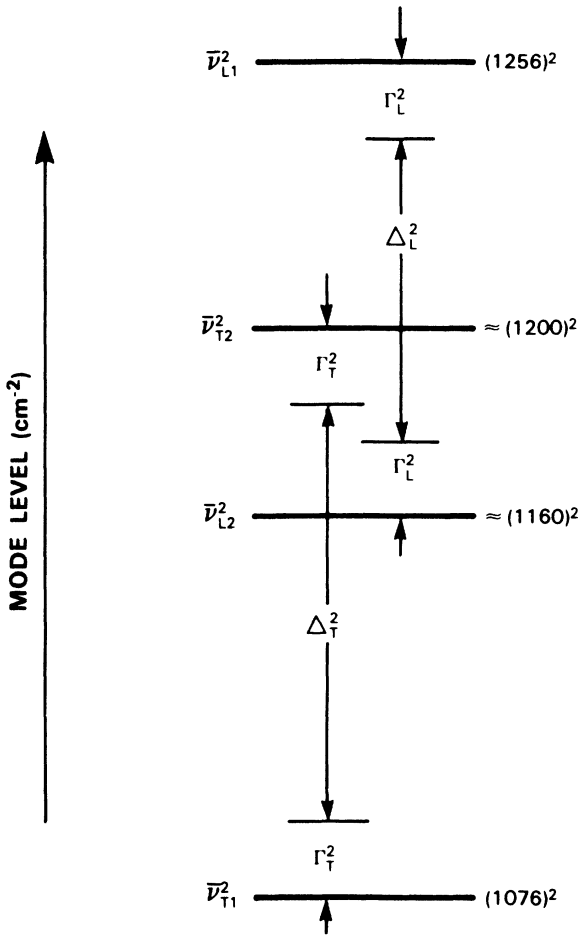

FIG. 9. Analytical model for the AS coupled-mode vibrational levels of a-SiO_2.

$$(1-2\Lambda_T^2)[1+(2\nu_{T12}^2/\Delta_T^2)^2]^{1/2}=1 \ . \tag{51}$$

Upon eliminating Δ_T^2 and ν_{T12}^2 from among Eqs. (46)–(51), the coupled-mode–model equations reduce to the relations

$$F_1=\frac{\epsilon_\infty}{4\pi}(\bar{\nu}_{L1}^2-\bar{\nu}_{T1}^2)\prod_{\substack{k=2\\(k\neq 1)}}^{N}\frac{\bar{\nu}_{Lk}^2-\bar{\nu}_{T1}^2}{\bar{\nu}_{Tk}^2-\bar{\nu}_{T1}^2} \tag{52}$$

and

$$F_2=\frac{\epsilon_\infty}{4\pi}(\bar{\nu}_{L2}^2-\bar{\nu}_{T2}^2)\prod_{\substack{k=1\\(k\neq 2)}}^{N}\frac{\bar{\nu}_{Lk}^2-\bar{\nu}_{T2}^2}{\bar{\nu}_{Tk}^2-\bar{\nu}_{T2}^2} \ , \tag{53}$$

where N is the number of modes. For the model of just the two mechanically coupled modes, $N=2$. However, because all LO modes of a system's split LO-TO pairs are coupled independent of whether they are mechanically coupled or not, as discussed in Sec. III D, N has been deliberately left unspecified in these equations in case the system contains additional split LO-TO-pair modes that are not mechanically coupled but need to be included due to longitudinal coupling.

Table II shows values of F_1 and F_2 calculated from Eqs. (52) and (53), respectively, using the values listed in the table for the frequencies of the four LO-TO pairs. As shown in Table II, there is good agreement between the calculated and measured value of F_1. No experimental intergrated absorption measurements for F_2 were made because the absorption peak for this mode is not well defined. However, since the overall strength of the coupled modes is conserved, the sum of the calculated values of F_1 and F_2 scaled to the density of quartz, approximately 60 580 cm^{-2}, can be compared to the sum of similar modes in quartz (the E modes with TO frequencies at 1072 and 1163 cm^{-1}). Spitzer's data[14] give $62\,350\pm1830$ cm^{-2} as the sum of the TO strengths for the two modes in quartz. The value for the sum of the TO-mode strengths derived from the thin a-SiO_2 film is within the error bounds of the value obtained from Spitzer's data. This supports the idea that, properly scaled, the combined TO-mode strength of the two AS modes is conserved with respect to crystalline quartz and a-SiO_2, and that comparative differences in the scaled separate strengths of these two modes in quartz and a-SiO_2 are due to increased coupling of the modes in a-SiO_2.

The coupled-mode model described by Eqs. (46)–(51) is underconstrained since the six equations contain seven unknown variables. As a result of this underconstraint, it can be shown that an arbitrary number of equivalent solutions for the coupled-mode model can be generated from the unitary matrix transformation U, which leaves ϵ_T^r, as given by Eq. (31), invariant, i.e.,

$$Q'=UQ \ , \tag{54}$$

$$G_T'=UG_T\tilde{U} \ , \tag{55}$$

where, for two coupled modes,

$$U=\begin{bmatrix}\cos\eta & \sin\eta\\ -\sin\eta & \cos\eta\end{bmatrix} , \tag{56}$$

and η is an arbitrary coupling angle such that $0\leq\eta<2\pi$. Consequently, while the model correctly relates mode strengths to the LO and TO frequencies of the various LO-TO split-pair modes [compare Eqs. (52) and (53) with Eq. (4)], details of the model, such as the values of the mechanical coupling coefficient Λ_T^2 and the effective charges Q_1 and Q_2, cannot be uniquely determined unless a value for one of the unknowns can be obtained independent of the model as applied to a-SiO_2.

Toward this end, an independent estimate of the unperturbed transverse level separation Δ_T^2 can be made from the AS_1 and AS_2 TO E-mode frequencies of α-quartz assuming the only difference in the actual transverse level separation $\bar{\nu}_{T2}^2$-$\bar{\nu}_{T1}^2$ of these modes in α-quartz and the same modes in a-SiO_2 is that ν_{T12}^2, the mechanical coupling between these modes, is zero in α-quartz. In this case the application of the coupled-mode model, Eq. (48), to α-quartz yields

$$\Delta_T^2=203\,400 \ cm^{-2} \ , \tag{57}$$

where the experimental values of the TO frequencies used for the AS_1 and AS_2 E modes of α-quartz were the nominal values $\bar{\nu}_{T2}=1163$ cm^{-1} and $\bar{\nu}_{T1}=1072$ cm^{-1}, respectively, given by Spitzer *et al.*[14]

Application of the modified coupled-mode model as given by Eqs. (46)–(51) and (57) to a-SiO_2 using the experimental data of Table II yields the following estimates for the values of the model parameters, all in units of cm^{-2}: a transverse coupling coefficient $\Lambda_T^2=0.140$ corresponding to a mechanical coupling parameter value for the model of $2\nu_{T12}^2=\pm195\,700$, and a pair of mathematically equivalent solutions for the values of the squared effective transverse charge parameters Q_1^2 and Q_2^2. One of the solutions yields the values $Q_1^2=55\,400$ and $Q_2^2=0.339$ such that if arbitrarily Q_1 is defined to be positive, then $Q_2>0$ for $\nu_{T12}^2>0$ and $Q_2<0$ for $\nu_{T12}^2<0$. The other solution yields the values $Q_1^2=28\,600$ and $Q_2^2=26\,800$ such that if again arbitrarily Q_1 is defined to be positive, then $Q_2<0$ for $\nu_{T12}^2>0$ and $Q_2>0$ for $\nu_{T12}^2<0$. Both solutions, used appropriately in Eqs. (49) and (50), produce the calculated values for F_1 and F_2 given in Table II once the effect of the charge coupling of additional dipolar modes is taken into account [as in Eqs. (52) and (53)] and the resulting values are scaled to the density of α-quartz.

Even though both solutions are equivalent under a unitary transformation and provide the same fit to the experimental data, the physical models described by these solutions are different. While the magnitude of Δ_T^2 is the same for each solution, the magnitudes and, depending on the sign of ν_{T12}^2, the relative signs of Q_1 and Q_2 are different. In the first solution described above, Q_2 is quite small compared to Q_1 and hence the optical activity of the AS modes is due almost entirely to the AS_1 mode and its two vibrational frequencies acquired as a result of its mechanical coupling to the optically inactive AS_2 mode. In the second solution, Q_1 and Q_2 are comparable in magnitude and hence both the AS_1 and the AS_2 modes are optically active. The disparity in the mode strengths at the two TO absorption levels of the two coupled modes

is the result of Q_1 and Q_2 being mixed additively at their lower vibrational frequency and subtractively at their higher vibrational frequency, as indicated in Eqs. (49) and (50).

From a mathematical point of view, unless and until there is some more information on the magnitude of Q_2 and its sign with respect to Q_1 in a-SiO_2, there is no way to choose the "correct" coupled-mode model from among these several models since they all equally fit the present data.

From the standpoint of physics, the simplicity and understandability of the first solution given above is to be preferred. Thus, in going from α-quartz to a-SiO_2, the only significant result of becoming amorphous is the introduction of mechanical coupling between the AS_1 and AS_2 modes. Also, from the nature of the AS_1 and AS_2 modes (adjacent AS dipoles vibrating in phase and 180° out of phase with each other, respectively), it can be understood, at least in the long-wavelength approximation, how Q_1 can have a large finite value while the value of Q_2 can be equal to zero or very nearly so.

VI. COMPARISON WITH OTHER ANALYSES

Some confusion exists in the literature as to the nature of the mode at 1200 cm^{-1} in a-SiO_2. It has been pointed out that while an analysis of the infrared-reflection spectra of silica revealed that one of its LO vibrational modes of should occur at approximately 1256 cm^{-1}, a peak in this region was absent from the Raman spectrum.[2,3] Accordingly, the infrared results obtained for silica were treated with some suspicion.[2] It was concluded in Ref. 2 that some error was made in the analysis of the infrared-reflectivity data, resulting in a spurious LO absorption peak at $\approx$1256 cm^{-1} and that the Raman peak at 1200 cm^{-1} is the site of the LO mode which is to be paired with the TO mode in the 1070-cm^{-1} region of the a-SiO_2 infrared spectrum. However, the hyper-Raman data of Ref. 3 for fused quartz and the Berreman-effect measurements of Refs. 7 and 8 and this paper on thin silica films confirm the infrared-reflectivity spectral result that the LO mode paired with the 1076-cm^{-1} TO mode of this paper lies at 1256 cm^{-1}. Furthermore, the mode at 1200 cm^{-1} must be a TO mode since it shows up in the TO component of the Berreman spectrum [Fig. 8(b)] and is required as a consequence of the interspersion of LO and TO modes (Sec. III D).

It is interesting to compare the experimental values for the positions of the four pairs of LO-TO-mode peaks listed in Table II for a-SiO_2 with the VDOS for a-SiO_2 as obtained by Carpenter and Price[34] from vitreous SiO_2 using coherent inelastic neutron scattering. The comparison is shown in Fig. 10. It can be seen from the figure that peaks in the VDOS generally tend to coincide with the peaks of the TO modes (solid vertical lines) rather than the LO-mode peaks (dashed vertical lines). This is especially obvious in the higher-frequency modes, where there tends to be less overlapping of the VDOS bands. In fact, judging from Fig. 10, there appear to be no prominent features in the VDOS spectrum that can be associated with the LO-mode peaks.

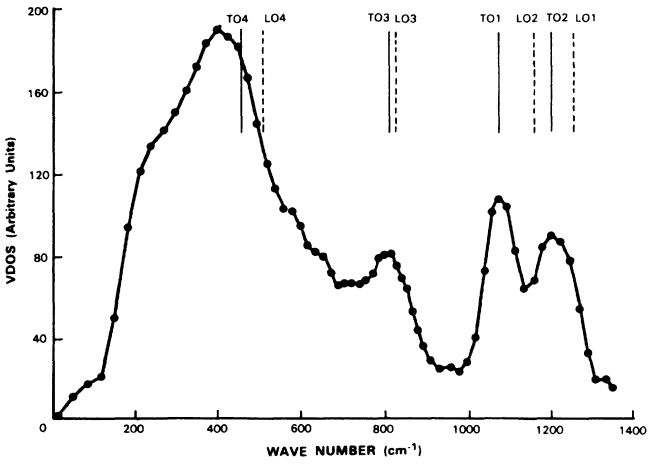

FIG. 10. Comparison of experimental values for the four pairs of LO-TO-mode absorption peaks (LOj-TOj, $j=1,\ldots,4$) of a-SiO_2 listed in Table II with the VDOS spectrum for a-SiO_2 as obtained by Carpenter and Price (Ref. 34) from vitreous SiO_2 using coherent inelastic neutron scattering. The positions of the LOj absorption peaks are indicated by vertical dashed lines, the TOj absorption peaks by vertical solid lines, and the experimental values of the VDOS spectral plot by solid circles (●) joined by straight lines to guide the eye.

This observation of the correspondence between the TO modes and peaks in the VDOS of a-SiO_2 agrees with theoretical results obtained by de Leeuw and Thorpe.[35] By including long- (infinite-) range Coulomb effects in a study of the vibrational properties of a computer-generated random network with the chemical formula AX_2, they provide calculated results showing for the first time unambiguous evidence for a LO-TO splitting in these systems. Because of the strong negative dispersion of the LO mode, de Leeuw and Thorpe found that LO-TO splitting does not give rise to a double peak in their calculated VDOS. Instead, they show that only a single VDOS peak is associated with the splitting of a vibrational mode into a LO-TO pair, and that in the long-wavelength limit this peak corresponds closely in frequency to their calculated TO peak. Furthermore, they show that in the long-wavelength limit their calculated LO peak occurs at a band edge in the VDOS, as is observed experimentally in Fig. 10. They go on to suggest that the extra (second) peak at $\approx$1200 cm^{-1} in the VDOS of Fig. 10 is due, as has been shown in this paper, to the relatively optically inactive AS_2 mode. According to de Leeuw and Thorpe, their random-network-model parameters would have to be further refined to produce this second peak.

Two high-frequency peaks in the calculated VDOS have been obtained from random-network models using only short-range interactions. Pick and Yvinec[36] obtained two peaks by considering tetrahedral glasses of the chemical form AX_2 as a dense assembly of AX_4 molecules with random but fixed positions coupled only by dipole-dipole interactions. They observed quite correctly that the dipole-dipole couplings produced a split-up simi-

lar to that found in the Raman spectrum of SiO_2,[1,2] but wrongly associated this with LO-TO splitting.[35] Guttman and Rahman,[37] using a continuous-random-network model of SiO_2 and a modified Keating potential[38] that included only short-range forces, observed a double peak at high frequencies in their calculated density of states. They also showed that the calculated density of states agrees fairly well with an experimental density of states obtained from inelastic-neutron-scattering data. Similarly, Lucovsky *et al.*,[5] using a refinement of the Bethe-lattice method including up to second-neighbor interactions to study a-SiO_2, obtained two peaks attributing them, as discussed earlier in Sec. IV B, to AS_1- and AS_2-type TO vibrational modes.

It is known that in amorphous solids the Raman spectrum tends to mimic the vibrational density of states,[39] especially at high frequencies.[1] Thus, it would appear from the foregoing discussion that the high-frequency doublet in the experimental Raman spectrum for a-SiO_2 is due to the same short-range interactions that give rise to the high-frequency AS_1 and AS_2 TO peaks in the VDOS spectrum shown in Fig. 10.

VII. CONCLUSIONS

In addition to the three well-known vibrational modes of a-SiO_2 with sufficient oscillator strength to show significant LO-TO splitting located at 507(LO)–457(TO), 820(LO)–810(TO), and 1256(LO)–1076(TO) cm^{-1}, there is a fourth mode exhibiting inverted LO-TO splitting at $\approx$1160(LO)–$\approx$1200(TO) cm^{-1}. The fourth mode, optically weak in crystalline α-quartz, owes its increased optical strength in a-SiO_2 to increased coupling between the AS_1 and AS_2 vibrational modes. The observed decrease in the strength of the AS_1 mode, 1256–1076 cm^{-1}, and the concomitant increase in the strength of the AS_2 mode, $\approx$1160–$\approx$1200 cm^{-1}, in a-SiO_2 compared to crystalline α-quartz is a direct result of the coupling.

LO-TO splitting of all four modes can be observed experimentally in the infrared-absorption spectra of very thin films of a-SiO_2 by making use of the Berreman effect. Neither the experimental VDOS nor the Raman spectrum portrays the observed LO-TO-mode splittings in a-SiO_2. Instead, the major peaks of these spectra, especially at the higher frequencies, align closely with the observed TO peaks. In fact, no significant feature of either spectrum appears to be associated with the experimental positions of the LO peaks, including the double maximum at high frequencies.

ACKNOWLEDGMENTS

The author is pleased to acknowledge useful discussions with Dr. Peter W. Wyatt and Professor Stephen D. Senturia of MIT. He also wishes to acknowledge Jeffrey M. Knecht for his assistance in obtaining the oxide films and taking the infrared spectra. This work was sponsored by the U.S. Department of the Air Force.

APPENDIX: INTERSPERSION ANALYSIS OF LO- AND TO-MODE LEVELS

LO- and TO-mode levels are related to each other even in the absence of the mechanical coupling coefficient ν_{T12}^2. It can be seen from Eq. (30) that the longitudinal coupling coefficient ν_{L12}^2 does not necessarily vanish when ν_{T12}^2 does. Coupling between longitudinal modes exists due to the interaction between the dipole charges associated with each of the two oscillator modes through the polarization-induced field term, $-4\pi P$, of Eqs. (25) and (26). In this appendix it is shown that this polarization-induced field coupling of the dipole charge (charge coupling) acts in such a manner as to ensure that a LO-mode level is always interspersed between any two successive TO-mode levels.

Two cases of interspersion of LO and TO modes are considered here. They are shown in Figs. 4(a) and 4(b). Each case involves two LO-TO-mode pairs for which there is no mechanical coupling between the modes and the higher-frequency TO mode is labeled the T22 mode. There are no restrictions as to the location of the uncoupled LO modes other than the normal one of lying higher in frequency than their respective TO mode.

For the case in which $\nu_{T12}^2=0$ and $\nu_{L22}^2(0)>\nu_{L11}^2(0)$, the relationship of the longitudinal mode levels with respect to the transverse levels is shown in Fig. 4(a) assuming $\nu_{T22}^2(0)>\nu_{T11}^2(0)$. The levels on the left-hand side of the figure, $\nu_{T11}^2(0)$, $\nu_{T22}^2(0)$, $\nu_{L11}^2(0)$, and $\nu_{L22}^2(0)$, are the transverse and longitudinal mode levels for $\nu_{L12}^2(0)=0$, i.e., the charge coupling between the two longitudinal modes is "off," the argument "0" indicating that $\nu_{L12}^2=0$. Differences between the longitudinal and transverse levels associated with each of the two oscillator modes $4\pi Q_1^2/\epsilon_\infty$ and $4\pi Q_2^2/\epsilon_\infty$ are the result of the self-interaction of the dipole oscillators through the polarization-induced field. Since these two terms are always greater than or equal to zero, Eq. (30) shows that the longitudinal level is always greater than or equal to its transverse. Upon "turning on" the charge coupling between the two modes, the longitudinal levels "repel" each other as shown in the figure with $\nu_{L11}^2(0)$ decreasing by an amount $\Gamma_L^2(0)$ to ν_{L11}^2 and $\nu_{L22}^2(0)$ increasing by the same amount to ν_{L22}^2. The quantity $\Gamma_L^2(0)$ is the longitudinal mode level coupling coefficient upon turning the charge-coupling term, $\nu_{L12}^2=4\pi Q_1 Q_2/\epsilon_\infty$, "on." From Eqs. (42) and (30) it can be shown to be expressed by the relation

$$2\Gamma_L^2(0)=\{[\Delta_L^2(0)]^2+(8\pi Q_1 Q_2/\epsilon_\infty)^2\}^{1/2}-\Delta_L^2(0)\ ,$$

where

$$\Delta_L^2(0)=\nu_{L22}^2(0)-\nu_{L11}^2(0)$$
$$=\Delta_T^2+4\pi Q_2^2/\epsilon_\infty-4\pi Q_1^2/\epsilon_\infty$$

and

$$\Delta_T^2=\nu_{T22}^2-\nu_{T11}^2\ .$$

For the lower longitudinal mode level ν_{L11}^2 to lie between the two transverse mode levels $\nu_{T22}^2>\nu_{T11}^2$ such that $\nu_{T22}^2>\nu_{L11}^2>\nu_{T11}^2$ requires that

$$\frac{4\pi}{\epsilon_\infty}Q_1^2 > \Gamma_L^2(0) > \frac{4\pi}{\epsilon_\infty}Q_1^2 - \Delta_T^2 .$$

Upon assuming that both $\Delta_L^2(0)>0$ and $\Delta_T^2>0$ are satisfied, it can be shown that the above inequality is always satisfied regardless of the values of the charges Q_1 and Q_2 or the spacing of the transverse levels Δ_T^2. Upon substituting the relation given above for $\Gamma_L^2(0)$ into the inequality, a little algebra reveals that

$$\frac{4\pi}{\epsilon_\infty}Q_1^2+\frac{4\pi}{\epsilon_\infty}Q_2^2+\Delta_T^2 > \left[\left[\left[\frac{4\pi}{\epsilon_\infty}Q_1^2-\frac{4\pi}{\epsilon_\infty}Q_2^2-\Delta_T^2\right]^2+4\left[\frac{4\pi}{\epsilon_\infty}Q_1^2\right]\left[\frac{4\pi}{\epsilon_\infty}Q_2^2\right]\right]^{1/2} > \frac{4\pi}{\epsilon_\infty}Q_1^2+\frac{4\pi}{\epsilon_\infty}Q_2^2-\Delta_T^2 .$$

The left-hand and middle terms of this inequality relation are always positive regardless of the values for $\Delta_T^2(>0)$, Q_1, and Q_2, while the right-hand term may be of either sign. When the right-hand term is negative, the right-hand inequality is automatically satisfied. When this right-hand term is positive, all the terms in the above inequality relation can be squared without invalidating the relation. A little additional algebraic manipulation involving the factoring of the difference of two squares results in an inequality relation of the form

$$\frac{4\pi}{\epsilon_\infty}Q_1^2\left[\frac{4\pi}{\epsilon_\infty}Q_2^2+\Delta_T^2\right] > \frac{4\pi}{\epsilon_\infty}Q_1^2\frac{4\pi}{\epsilon_\infty}Q_2^2 > \left[\frac{4\pi}{\epsilon_\infty}Q_1^2-\Delta_T^2\right]\frac{4\pi}{\epsilon_\infty}Q_2^2 .$$

This last inequality is seen to be satisfied for all allowed values of Δ_T^2, Q_1, and Q_2. Accordingly, for $\nu_{T12}^2=0$ and $\nu_{L22}^2(0)>\nu_{L11}^2(0)$, the longitudinal mode level ν_{L11}^2 must always lie between the two transverse levels $\nu_{T22}^2>\nu_{T11}^2$ such that the inequality $\nu_{T22}^2>\nu_{L11}^2>\nu_{T11}^2$ is satisfied.

Similarly, for the case in which $\nu_{T12}^2=0$ and $\nu_{L11}^2(0)>\nu_{L22}^2(0)$, the relation between the longitudinal mode levels and the transverse levels is shown in Fig. 4(b), again assuming $\nu_{T22}^2(0)>\nu_{T11}^2(0)$. As before, "turning on" $\nu_{L12}^2=4\pi Q_1Q_2/\epsilon_\infty$ causes the longitudinal levels to "repel" each other as shown in the figure, with $\nu_{L22}^2(0)$ decreasing by an amount $\Gamma_L^2(0)$ to ν_{L22}^2, and $\nu_{L11}^2(0)$ increasing by the same amount to ν_{L11}^2. The longitudinal mode level coupling coefficient $\Gamma_L^2(0)$ is still given by

$$2\Gamma_L^2(0)=\{[\Delta_L^2(0)]^2+(8\pi Q_1Q_2/\epsilon_\infty)^2\}^{1/2}-\Delta_L^2(0) ,$$

but now

$$\Delta_L^2(0)=\nu_{L11}^2(0)-\nu_{L22}^2(0)$$
$$=4\pi Q_1^2/\epsilon_\infty-4\pi Q_2^2/\epsilon_\infty-\Delta_T^2$$

and

$$\Delta_T^2=\nu_{T22}^2-\nu_{T11}^2 .$$

For the lower longitudinal mode level ν_{L22}^2 to lie between the two transverse mode levels $\nu_{T22}^2>\nu_{T11}^2$ such that $\nu_{T22}^2>\nu_{L22}^2>\nu_{T11}^2$ requires that

$$\frac{4\pi}{\epsilon_\infty}Q_2^2+\Delta_T^2 > \Gamma_L^2(0) > \frac{4\pi}{\epsilon_\infty}Q_2^2 .$$

As before, a little algebraic manipulation and some factoring reduces this inequality to

$$\frac{4\pi}{\epsilon_\infty}Q_1^2\left[\frac{4\pi}{\epsilon_\infty}Q_2^2+\Delta_T^2\right] > \frac{4\pi}{\epsilon_\infty}Q_1^2\frac{4\pi}{\epsilon_\infty}Q_2^2 > \left[\frac{4\pi}{\epsilon_\infty}Q_1^2-\Delta_T^2\right]\frac{4\pi}{\epsilon_\infty}Q_2^2 ,$$

which is seen to be satisfied for all allowed values of Δ_T^2, Q_1, and Q_2. Thus, for $\nu_{T12}^2=0$ and $\nu_{L11}^2(0)>\nu_{L22}^2(0)$, the longitudinal mode level ν_{L22}^2 must always lie between the two transverse levels $\nu_{T22}^2>\nu_{T11}^2$ such that the inequality $\nu_{T22}^2>\nu_{L22}^2>\nu_{T11}^2$ is satisfied. Interestingly, ν_{L22}^2 is lower in value than ν_{T22}^2. Normally, the LO-mode level of a LO-TO pair lies above the TO-mode level in value; however, when both levels of an LO-TO pair are intermediate between the levels of another LO-TO pair, then the levels of the intermediate pair are reversed, as in the case just discussed.

[1]For a recent discussion and additional references, see F. L. Galeener, A. J. Leadbetter, and M. W. Stringfellow, Phys. Rev. B **27**, 1052 (1983).

[2]F. L. Galeener and G. Lucovsky, Phys. Rev. Lett. **37**, 1474 (1976).

[3]V. N. Denisov, B. N. Mavrin, V. B. Podobedov, and Kh. E. Sterin, Fiz. Tverd. Tela (Leningrad) **20**, 3485 (1978) [Sov. Phys.—Solid State **20**, 2016 (1978)].

[4]G. Jungk and A. Röseler, Phys. Status Solidi B **124**, K1 (1984).
[5]G. Lucovsky, C. K. Wong, and W. B. Pollard, J. Non-Cryst. Solids **59&60**, 839 (1983).
[6]P. G. Pai, S. S. Chao, Y. Takagi, and G. Lucovsky, J. Vac. Sci. Technol. A **4**, 689 (1986).
[7]K. Hübner *et al.*, Phys. Status Solidi B **104**, K1 (1981).
[8]B. Harbecke, B. Heinz, and P. Grosse, Appl. Phys. A **38**, 263 (1985).
[9]D. W. Berreman, Phys. Rev. **130**, 2193 (1963).
[10]F. Seitz, *The Modern Theory of Solids* (McGraw-Hill, New York, 1940), Chap. 17.
[11]M. Behmer and R. Claus, Phys. Rev. **30**, 4800 (1984).
[12]M. L. Naiman *et al.*, J. Electrochem. Soc. **131**, 637 (1984).
[13]M. L. Naiman *et al.*, J. Appl. Phys. **58**, 779 (1985).
[14]W. G. Spitzer and D. A. Kleinman, Phys. Rev. **121**, 1324 (1961).
[15]A. S. Baker, Jr., Phys. Rev. **136**, A1290 (1964).
[16]M. V. Belousov, Fiz. Tverd. Tela (Leningrad) **15**, 1206 (1973) [Sov. Phys.—Solid State **15**, 813 (1973)].
[17]P. Grosse *et al.*, Appl. Phys. A **39**, 257 (1986).
[18]S. Maeda, G. Thyagarajan, and P. N. Schatz, J. Chem. Phys. **39**, 3474 (1963).
[19]In the older notation of Ref. 14, $F_j=\rho_j\nu_j^2$.
[20]J. F. Scott and S. P. S. Porto, Phys. Rev. **161**, 903 (1967).
[21]P. H. Gaskell and D. W. Johnson, J. Non-Cryst. Solids **20**, 153 (1976).
[22]P. H. Gaskell and D. W. Johnson, J. Non-Cryst. Solids **20**, 171 (1976).
[23]In the notation of Ref. 21, $F_j=\Delta\epsilon_j\nu_j^2/4\pi$.
[24]W. A. Pliskin and R. P. Esch, Appl. Phys. Lett. **11**, 257 (1967).
[25]Because of the finite thickness of Pliskin's oxide film ($\simeq$136 nm), the value of F_1 obtained using Eq. (16) without taking the limit is only approximate.
[26]A. S. Baker, Jr. and J. J. Hopfield, Phys. Rev. **135**, A1732 (1964).
[27]E. Burstein, S. Iwasa, and Y. Sawada, in *Proceedings of the E. Fermi International School of Physics, Course XXXIV, Optical Properties of Solids, Varenna, 1965,* edited by J. Tauc (Academic, New York, 1966).
[28]With no mechanical coupling there is no need to distinguish between coupled and uncoupled TO modes.
[29]F. McCrackin, *A Fortran Program for the Analysis of Ellipsometer Measurements,* National Bureau of Standards Technical Note No. 479 (U.S. GPO, Washington, D.C., 1969).
[30]A. Savitzky and M. J. E. Golay, Anal. Chem. **36**, 1627 (1964).
[31]H. R. Philipp, J. Appl. Phys. **50**, 1053 (1979).
[32]F. A. Johnson, Proc. Phys. Soc. London **73**, 265 (1959).
[33]P. Flubacher, A. J. Leadbetter, J. A. Morrison, and B. P. Stoicheff, J. Phys. Chem. Solids **12**, 53 (1959).
[34]J. M. Carpenter and D. L. Price, Phys. Rev. Lett. **54**, 441 (1985).
[35]S. W. de Leeuw and M. F. Thorpe, Phys. Rev. Lett. **55**, 2879 (1985).
[36]R. M. Pick and M. Yvinec, in *Proceedings of the International Conference on Lattice Dynamics, Paris, 1977,* edited by M. Balkanski (Flammarion, Paris, 1977), p. 459.
[37]L. Guttman and S. Rahman, J. Non-Cryst. Solids **75**, 419 (1985).
[38]P. N. Keating, Phys. Rev. **145**, 637 (1966).
[39]R. Shuker and R. W. Gammon, Phys. Rev. Lett. **25**, 222 (1970).